Journal of Neuroinflammation

BioMed Central

Research

Open Access

Intradermal administration of magnesium sulphate and magnesium chloride produces hypesthesia to mechanical but hyperalgesia to heat stimuli in humans

Takahiro Ushida*[1,2,3], Osamu Iwatsu[2], Kazuhiro Shimo[1], Tomoko Tetsunaga[2], Masahiko Ikeuchi[2], Tatsunori Ikemoto[2,3], Young-Chang P Arai[1], Katsutoshi Suetomi[1] and Makoto Nishihara[1]

Address: [1]Multidisciplinary Pain Center, Aichi Medical University, 21 Karimata, Yazako, Nagakute, Aichi 480-1195, Japan, [2]Department of Orthopaedic Surgery, Kochi Medical School, Kohasu, Okoh-cho, Nankoku, Kochi 783-8505, Japan and [3]Nankoku Pain Research Group, Kochi Medical School, Kohasu, Okoh-cho, Nankoku, Kochi 783-8505, Japan

Email: Takahiro Ushida* - ushidat-koc@umin.ac.jp; Osamu Iwatsu - hcb03073@nifty.com; Kazuhiro Shimo - xia@oct.zaq.ne.jp; Tomoko Tetsunaga - tt1201@softbank.ne.jp; Masahiko Ikeuchi - ikeuchim@kochi-u.ac.jp; Tatsunori Ikemoto - tatsunon31@hotmail.com; Young-Chang P Arai - arainon@aichi-med-u.ac.jp; Katsutoshi Suetomi - suetomi-dm@umin.ac.jp; Makoto Nishihara - nisihara@aichi-med-u.ac.jp

* Corresponding author

Published: 28 August 2009

Journal of Neuroinflammation 2009, **6**:25 doi:10.1186/1742-2094-6-25

Received: 29 April 2009
Accepted: 28 August 2009

This article is available from: http://www.jneuroinflammation.com/content/6/1/25

Abstract

Background: Although magnesium ions (Mg^{2+}) are known to display many similar features to other 2+ charged cations, they seem to have quite an important and unique role in biological settings, such as NMDA blocking effect. However, the role of Mg^{2+} in the neural transmission system has not been studied as sufficiently as calcium ions (Ca^{2+}). To clarify the sensory effects of Mg^{2+} in peripheral nervous systems, sensory changes after intradermal injection of Mg^{2+} were studied in humans.

Methods: Magnesium sulphate, magnesium chloride and saline were injected into the skin of the anterior region of forearms in healthy volunteers and injection-induced irritating pain ("irritating pain", for short), tactile sensation, tactile pressure thresholds, pinch-pain changes and intolerable heat pain thresholds of the lesion were monitored.

Results: Flare formation was observed immediately after magnesium sulphate or magnesium chloride injection. We found that intradermal injections of magnesium sulphate and magnesium chloride transiently caused irritating pain, hypesthesia to noxious and innocuous mechanical stimulations, whereas secondary hyperalgesia due to mechanical stimuli was not observed. In contrast to mechanical stimuli, intolerable heat pain-evoking temperature was significantly decreased at the injection site. In addition to these results, spontaneous pain was immediately attenuated by local cooling.

Conclusion: Membrane-stabilizing effect and peripheral NMDA-blocking effect possibly produced magnesium-induced mechanical hypesthesia, and extracellular cation-induced sensitization of TRPV1 channels was thought to be the primary mechanism of magnesium-induced heat hyperalgesia.

Background

Although magnesium ions (Mg^{2+}) are widely distributed throughout the whole organ, the role of Mg^{2+} in the neural transmission system has not been studied as sufficiently as calcium ions (Ca^{2+}). Much research has mentioned that Mg^{2+} shows a similar physiological attitude to Ca^{2+} and it has been reported that both ions have a membrane-stabilizing effect on nerves [1,2]. In addition, Mg^{2+} is known to act as a competitor to Ca^{2+}, in extracellular matrix [3]. However, the specific role of Mg^{2+} in neurophysiological transmission, especially concerning peripheral somatosensory systems, has been insufficiently focused on and not understood enough.

Among the various studies, the noncompetitive antagonistic action of Mg^{2+} on N-methyl-D-aspartate (NMDA) receptor, a glutamate receptor, was the focus of various reports [4]. Although the role of spinally-located NMDA receptors has been the focus of pain-related research before, NMDA receptors are also known to exist in peripheral nervous system [5]. Carlton et al. reported an increased population of peripheral glutamate receptors in injured peripheral nerve tissue [6]. In a previous study, Iwatsu et al. reported that intradermal administration of NMDA receptor antagonists, ketamin hydrochloride and magnesium sulphate, produces hypesthesia to mechanical stimuli in humans [7]. Therefore, Mg^{2+} may alter neuronal activities both centrally and peripherally.

Concerning therapeutic effects, magnesium sulphate is known to improve types of pain in humans and animals [8]. On the other hand, Mikkelsen et al. reported that intravenous injection of Mg^{2+} (magnesium sulphate) produces heat hyperalgesia in humans [9].

Since much previous research has reported contradictory results, it is necessary to organize human investigation to clarify real changes of sensory experiences after administrations of Mg^{2+}. In our healthy volunteer study, subjects were asked to estimate the degree of pain and the effect of the drug was examined. In addition to noxious mechanical stimulation and noxious radiant heat stimulation, we performed an experiment evaluating innocuous mechanical stimulation, such as tactile sensation, in order to investigate the effect of intradermally applied magnesium sulphate (MS) and magnesium chloride (MC).

Methods

Fifteen healthy volunteers (age ranged from 26 to 34 years, mean: 29 years) were enrolled in sensory testing study after intradermal injection of magnesium ions and another 15 healthy volunteers (age ranged from 22 to 43 years, mean: 28 years) were enrolled in the experiment for examining the effect of local cooling in Mg^{2+} ion induced irritating pain study. All protocols were conducted in accordance with the recommendations outlined in the Declarations of Helsinki and were approved by the local Medical Ethical Committee. All subjects agreed to the study protocols and signed an informed consent form prior to the examination.

Sensory testing study after intradermal injection of magnesium ion

Using the double-blind method, each subject (n = 15) received one intradermal injection of 0.5 M MS (0.1 ml, 524 mOSM) into one anterior ulnar site on the forearm and one injection of physiological saline (0.1 ml, 0.9% NaCl, 290 mOSM) at the same site into the other forearm as a control. At least one week after injection of 0.5 M MS, the same subjects received one injection of 0.05 M MS (0.1 ml, 337 mOSM) and saline in the same way. With 0.05 M MC and physiological saline solutions, they were injected with MC (0.1 ml, 385 mOSM) and physiological saline (0.1 ml) under the same procedure at least one week later. Therefore, each subject received one injection of 0.5 M & 0.05 M MS, and 0.05 M MC, and three injections of saline. Following injection, the resulting effects were evaluated after 1, 10, 20, 30, 45 and 60 min. for the MS site, MC site and NaCl site. The following tests were undertaken in a quiet room and room temperature was maintained at 25°C. Skin surface around the injection (test) area was kept at 34°C by servo-controlled thermal controller (Dantec Dynamics, Skovlunde, Denmark).

Injection-induced irritating pain evaluation

The intensity of irritating pain was evaluated by 100 mm visual analogue scale ('VAS') before and after injection of test solutions.

Tactile sensation evaluation

Using a horse hair brush, tactile sensations at the wheal region formed by intradermal injection and the region of unaffected skin were compared. Rating the sense of normal skin on the same arm as 10, the tactile sensation at the wheal region was evaluated using a numeric rating scale ('NRS').

Tactile pressure threshold test

Using the von Frey filaments, the tactile pressure threshold in intradermally injected area was measured. Prior to this experiment, pressure force of each von Frey filament was calibrated.

Pinch-pain evaluation test

Using an arterial clamp, the pain intensity evoked by pinch at the wheal region formed by intradermal injection and unaffected normal proximal skin were compared. Rating the sense of pain of normal skin on the same arm as 10, the pain intensity at the wheal region was evaluated using NRS. In addition, same pinch (noxious mechanical)

stimulations were applied to the skin, located 1 cm apart from wheal region to check existence of secondary hyperalgesia.

Measurement of intractable heat pain evoking temperature

Thermal stimulation was applied by Peltier probe controller (Intercross-200, Intercross Co., Tokyo, Japan). Tip of the probe (2.5 × 2.5 cm) was applied to injection site and temperature of the probe was serially increased from 30 to 50°C (+0.5°C/sec.). Experimental subjects were instructed to push a button when they experienced intolerant heat pain sensation (The threshold temperature that induces intolerable heat pain). After pushing the button, the temperature of the probe was programmed to automatically return quickly to 30°C.

Changes in injection-induced irritating pain after cooling

After intradermal administration of MS (0.5 M), graded cooling stimuli (from 25 to 9°C: -0.5 - -2.1°C/sec) were applied to the injection site by Peltier probe controller (UDH-300, Unique Medical Co., Tokyo, Japan) (Fig. 1) and the intensity of irritating pain at each test temperature was recorded by NRS.

Statistical Analysis

All data are expressed as mean ± S.E.M Significant changes over time were determined with the Friedman's analysis of variance by ranks followed by post hoc pairwise comparisons.

Results

Local observation and injection-induced irritating pain evaluation

All test solutions containing Mg^{2+} produced flare formation around the injection site and irritating pain. The intensity of irritating pain evaluated by VAS showed a significant increase at 1-10 min after the injection of 0.5 M and 0.05 M MS. Furthermore, MC produced irritating pain at 1 min after injection. (Fig. 2A)

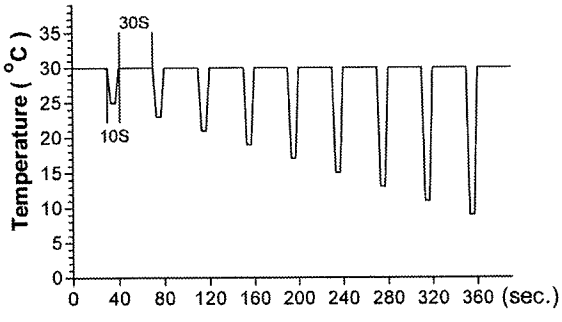

Figure 1
Schematic diagram of the graded cooling stimuli. To check changes in spontaneous pain appearing at the injection site, Peltier probe was directly attached to the injection site and cooled the skin in gradual increments.

Tactile sensation evaluation

After injection of MS, tactile sensation caused by brush decreased up to 20 min and by 1-10 min after injection of 0.5 M and 0.05 M MS respectively, and by 1-10 min after injection of 0.05 M MC (Fig. 2B) compared with the control level.

Tactile pressure threshold test

The tactile pressure threshold measured using the von Frey filaments significantly increased up to 20 min and by 1-10 min after injection of 0.5 M and 0.05 M MS respectively, and up to 20 min after injection of MC compared with saline. (Fig. 2C)

Pinch-pain evaluation test

The pinch-pain evoked by an arterial clamp was reduced up to 10 min after injection of 0.5 M and 0.05 M MS. Similar but shorter changes were observed after injection of MC. (Fig. 2D)

In addition apparent secondary hyperalgesia was not detected in flare area.

Measurement of intolerable heat pain evoking temperature

The threshold temperature that induces intolerable heat pain was decreased up to 20 min and by 1-10 min after intradermal injection of 0.5 M and 0.05 M MS respectively. Similarly MC decreased the pain evoking temperature up to 20 min after injection.

In contrast, intradermal injection of saline did not alter the intolerable heat pain threshold. (Fig. 3)

Effect of local cooling in Mg^{2+} ion-induced irritating pain

Cooling of the surface of the injected area apparently attenuated irritating pain. (Fig. 4) Furthermore, local flare did not change after local cooling.

Discussion

In the present study, both MS and MC solutions but not saline, inhibited the sensations evoked by noxious and innocuous mechanical stimuli but produced irritating pain. Several possible mechanisms can explain the Mg^{2+} ion-induced mechanical hypesthesia. As a general effect of the excitable membrane, changes in external divalent cations are considered to alter membrane surface potential and therefore, a high concentration of Mg^{2+} may inhibit the excitability of the axon by raising the electrical threshold of the membrane directly [2,10]. In pain-related poly-

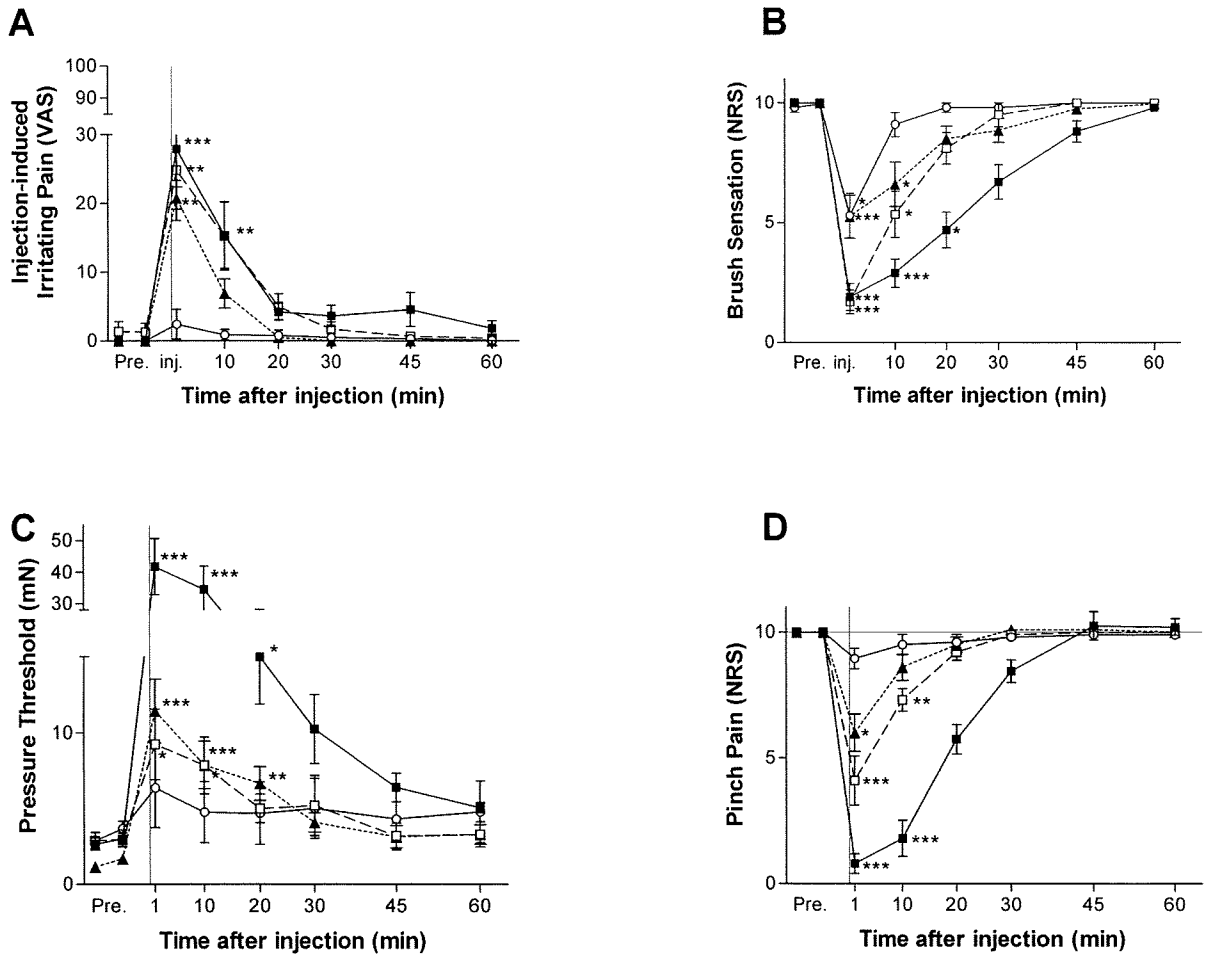

Figure 2
Time course of changes in effect of magnesium ion on pain and sensations. Fifteen volunteers were intradermally injected with 0.5 M $MgSO_4$ (black square), 0.05 M $MgSO_4$ (white square), 0.05 M $MgCl_2$ (black triangle), or saline (white circle). Each volunteer was injected with three kinds of magnesium solution at intervals of at least one week. Local spontaneous pain (A) was reported by visual analogue scale (VAS), Tactile sensation (B) and pinch pain intensity (D) were reported by a numerical rating score (NRS). When $MgSO_4$ and $MgCl_2$ solutions were injected, transient irritating pain and local hypesthesia to mechanical stimuli appeared at the injection site. *$p < 0.05$ vs. control; **$p < 0.01$ vs. control, ***$p < 0.001$ vs. control. As values were similar among these three saline injections, we have put the representative data herein.

modal receptors, Sato et al. showed that reduction of extracellular Ca^{2+} augmented the neuronal responses caused by hypertonic saline and high K solutions and also showed the augmented neuronal responses returned to control levels by an addition of Mg^{2+}, which suggests Mg^{2+} has a similar membrane-stabilizing effect on nerves to Ca^{2+}[11].

In addition, Chaban indicated that NMDA receptors on the periphery are involved in the transmission of noxious mechanical stimulation [12]. Only little attention has being paid so far to the functional importance of the peripherally-distributed NMDA receptors [7]. In a previous study, Ushida et al. evaluated the importance of mechanical stimulation by studying the relationship between magnesium ions and peripheral NMDA receptors [13]. It was found that injection of MK-801, an NMDA receptor antagonist, into the peripheral skin of rats produces inhibition of the sensations induced by innocuous and noxious stimulation.

Paradoxically, present results have shown that local administration of Mg^{2+} induces heat hyperalgesia, but mechanical hypesthesia at the injection site. Only a few

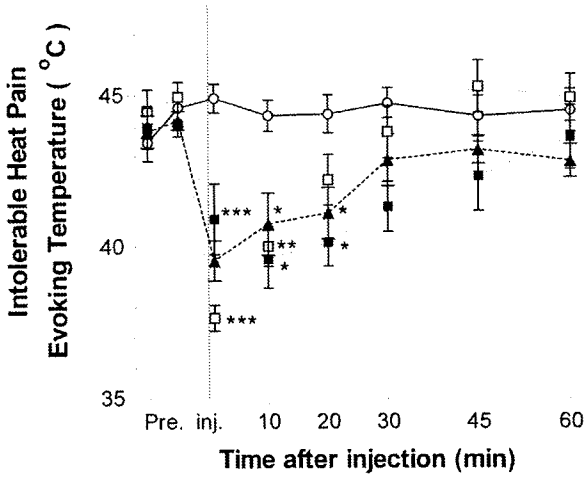

Figure 3
Time course of changes in intolerable heat pain evoking temperature after intradermal injection of magnesium solution. Fifteen volunteers were intradermally injected with 0.5 M $MgSO_4$ (black square), 0.05 M $MgSO_4$ (white square), 0.05 M $MgCl_2$ (black triangle), or saline (white circle). Each volunteer was injected with three kinds of magnesium solution at intervals of at least one week. Intolerant heat pain temperature was decreased at least 10 min following local administration of Mg^{2+}. *p < 0.05 vs. control; **p < 0.01 vs. control, ***p < 0.001 vs. control. As values were similar among these three saline injections, we have put the representative data herein.

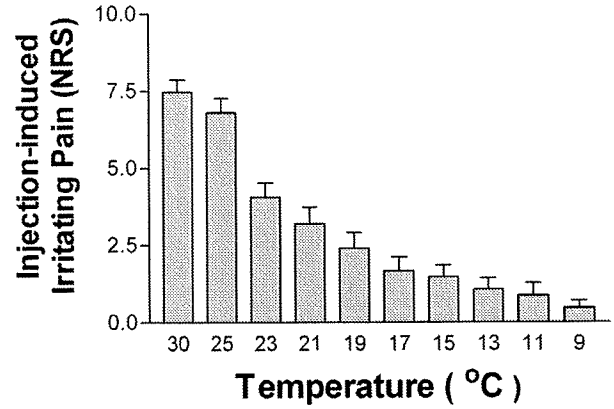

Figure 4
Changes in experienced pain intensity by local cooling. After intradermal administration of 0.5 M $MgSO_4$, Peltier probe was directly attached to the injection site. Pain intensity was substantially attenuated according to the cooling temperature. (n = 15)

researchers have paid attention to changes in Mg^{2+} -induced thermal sensations. Oral administration [14] and intrathecal injection [15] of magnesium sulphate are reported to improve heat hyperalgesia in animal models of neuropathic pain. On the other hand, Mikkelsen et al. reported that intravenous infusion of magnesium had no analgesic effect on thermal sensation in hyperalgesic skin but produced a decreased heat detection threshold and increased pain caused by 1 min long 45°C heat stimulation [9]. Since we could not find any sensory changes outside of wheals, peripheral mechanisms were suggested to explain magnesium-induced heat hyperalgesia.

Recently, transient receptor potential cation channel, subfamily V, member 1 (TRPV1), a heat-sensitive ion channel, has been discovered [16] and the role of this channel may be implicated in Mg^{2+}-induced heat hyperalgesia observed in our study. Indeed, Ahern et al. showed extracellular cations such as Na^+, Ca^{2+}, Mg^{2+} modulate/open the gates of TRPV1 channel by in vitro whole cell and single channel patch-clamp recording studies [17]. In addition to this direct mechanism, several neuropeptides and inflammatory mediators may be implicated in the enhanced activation of TRPV1. The flare formation observed at the injection site suggesting existence of axonal reflex-induced neuropeptide (SP, CGRP, etc) release from sensory nerve endings and released SP may result in sensitizing TRPV1 via activation of NK1, a SP receptor [18]. Also these inflammatory processes may activate the production of bradykinin (BK), a novel algesic substance. Increased extracellular concentration of BK results in sensitization and activates TRPV1 currents via PLC, PKC, and lipoxygenase-derived products [19-21].

These previous studies suggest that TRPV1 may be implicated in Mg^{2+} -induced hyperalgesia. Since cooling is known to desensitize local TRPV1, attenuation of Mg^{2+} -induced irritating pain by local cooling observed in our present study may also be explained by this mechanism.

Recently, types of thermal-sensing receptors such as TRPM8 (Transient receptor potential cation channel, subfamily M, member 8: cool receptor), TRPA1 (transient receptor potential cation channel, member A1: cold receptor), etc. have been discovered after TRPV1 and have been widely investigated [22,23]. In clinical settings, various types of diseases and patients possess the symptoms of thermal (heat, cold) hyperalgesia. However, it has been problematic under such settings to specify the underlying pathological mechanisms in these patients. Presumably, expression or activation of these recently discovered thermal receptors may play a key role in thermal pain and further translational research is necessary for the understanding and treatment of these intractable pain syndromes.

Conclusion

Intradermal administration of magnesium ions locally affected sensory systems and produced spontaneous pain, hypesthesia to both noxious and innocuous mechanical stimuli, and decreased the heat pain threshold. Activation of TRPV1 channel is the suggested mechanism for the development of heat hyperalgesia.

Abbreviations

MS: magnesium sulphate; MC: magnesium chloride; NMDA: N-methyl-D-aspartate; TRPV1: transient receptor potential cation channel, subfamily V, member 1; SP: substance P; CGRP: calcitonin gene-related peptide; NK-1: neurokinin 1; BK: bradykinin; PLC: phospholipase C; PKC: protein kinase C; TRPM8: transient receptor potential cation channel, subfamily M, member 8; TRPA1: transient receptor potential cation channel, member A1

Competing interests

The authors declare that they have no competing interests.

Authors' contributions

TU conceived of the study, participated in its study, and conducted all experiments. OI, KS (Shimo) and TT conducted the acquisition of data. MI and TI performed the statistical analysis. YAP, MN and KS (Suetomi) helped to draft the manuscript. All authors read and approved the final manuscript.

Acknowledgements

The authors would like to express their gratitude to Professor T. Tani and Dr. J. Sato for their invaluable comments on the manuscript and to Ms. Taki for technical assistance.

References

1. Fawcett WJ, Haxby EJ, Male DA: **Magnesium: physiology and pharmacology.** *Br J Anaesth* 1999, **83**:302-320.
2. Frankenhaeuser B, Hodgkin AL: **The action of calcium on the electrical properties of squid axons.** *J Physiol* 1957, **137**:218-244.
3. Hubbard JI, Jones SF, Landau EM: **On the mechanism by which calcium and magnesium affect the release of transmitter by nerve impulses.** *J Physiol* 1968, **196**:75-86.
4. Gean PW, Shinnick-Gallagher P: **Epileptiform activity induced by magnesium-free solution in slices of rat amygdala: antagonism by N-methyl-D-aspartate receptor antagonists.** *Neuropharmacology* 1988, **27**:557-562.
5. Coggeshall RE, Carlton SM: **Ultrastructural analysis of NMDA, AMPA, and kainate receptors on unmyelinated and myelinated axons in the periphery.** *J Comp Neurol* 1998, **391**:78-86.
6. Carlton SM, Coggeshall RE: **Inflammation-induced changes in peripheral glutamate receptor populations.** *Brain Res* 1999, **820**:63-70.
7. Iwatsu O, Ushida T, Tani T, Nada Bashir L, Yamamoto H: **Peripheral Administration of Magnesium Sulfate and Ketamine Hydrochloride Produces Hypesthesia to Mechanical Stimuli in Humans.** *Journal of health science* 2002, **48**:69-72.
8. Dube L, Granry JC: **The therapeutic use of magnesium in anesthesiology, intensive care and emergency medicine: a review.** *Can J Anaesth* 2003, **50**:732-746.
9. Mikkelsen S, Dirks J, Fabricius P, Petersen KL, Rowbotham MC, Dahl JB: **Effect of intravenous magnesium on pain and secondary hyperalgesia associated with the heat/capsaicin sensitization model in healthy volunteers.** *Br J Anaesth* 2001, **86**:871-873.
10. Hahin R, Campbell DT: **Simple shifts in the voltage dependence of sodium channel gating caused by divalent cations.** *J Gen Physiol* 1983, **82**:785-805.
11. Sato J, Mizumura K, Kumazawa T: **Effects of ionic calcium on the responses of canine testicular polymodal receptors to algesic substances.** *J Neurophysiol* 1989, **62**:119-125.
12. Chaban VV, Li H, Ennes HS, Nie J, Mayer EA, McRoberts JA: **N-methyl-D-aspartate receptors enhance mechanical responses and voltage-dependent Ca^{2+} channels in rat dorsal root ganglia neurons through protein kinase C.** *Neuroscience* 2004, **128**:347-357.
13. Ushida T, Tani T, Kawasaki M, Iwatsu O, Yamamoto H: **Peripheral administration of an N-methyl-D-aspartate receptor antagonist (MK-801) changes dorsal horn neuronal responses in rats.** *Neurosci Lett* 1999, **260**:89-92.
14. Hasanein P, Parviz M, Keshavarz M, Javanmardi K, Mansoori M, Soltani N: **Oral magnesium administration prevents thermal hyperalgesia induced by diabetes in rats.** *Diabetes Res Clin Pract* 2006, **73**:17-22.
15. Xiao WH, Bennett GJ: **Magnesium suppresses neuropathic pain responses in rats via a spinal site of action.** *Brain Res* 1994, **666**:168-172.
16. Tominaga M, Caterina MJ, Malmberg AB, Rosen TA, Gilbert H, Skinner K, Raumann BE, Basbaum AI, Julius D: **The cloned capsaicin receptor integrates multiple pain-producing stimuli.** *Neuron* 1998, **21**:531-543.
17. Ahern GP, Brooks IM, Miyares RL, Wang XB: **Extracellular cations sensitize and gate capsaicin receptor TRPV1 modulating pain signaling.** *J Neurosci* 2005, **25**:5109-5116.
18. Zhang H, Cang CL, Kawasaki Y, Liang LL, Zhang YQ, Ji RR, Zhao ZQ: **Neurokinin-1 receptor enhances TRPV1 activity in primary sensory neurons via PKCepsilon: a novel pathway for heat hyperalgesia.** *J Neurosci* 2007, **27**:12067-12077.
19. Premkumar LS, Ahern GP: **Induction of vanilloid receptor channel activity by protein kinase C.** *Nature* 2000, **408**:985-990.
20. Chuang HH, Prescott ED, Kong H, Shields S, Jordt SE, Basbaum AI, Chao MV, Julius D: **Bradykinin and nerve growth factor release the capsaicin receptor from PtdIns(4,5)P2-mediated inhibition.** *Nature* 2001, **411**:957-962.
21. Shin J, Cho H, Hwang SW, Jung J, Shin CY, Lee SY, Kim SH, Lee MG, Choi YH, Kim J, Haber NA, Reichling DB, Khasar S, Levine JD, Uhtaek Oh: **Bradykinin-12-lipoxygenase-VR1 signaling pathway for inflammatory hyperalgesia.** *Proc Natl Acad Sci USA* 2002, **99**:10150-10155.
22. Obata K, Katsura H, Mizushima T, Yamanaka H, Kobayashi K, Dai Y, Fukuoka T, Tokunaga A, Tominaga M, Noguchi K: **TRPA1 induced in sensory neurons contributes to cold hyperalgesia after inflammation and nerve injury.** *J Clin Invest* 2005, **115**:2393-2401.
23. Tominaga M, Caterina MJ: **Thermosensation and pain.** *J Neurobiol* 2004, **61**:3-12.

Neuroscience Letters 454 (2009) 97–100

Contents lists available at ScienceDirect

Neuroscience Letters

journal homepage: www.elsevier.com/locate/neulet

Changes in calcitonin gene-related peptide expression following joint immobilization in rats

Tomohiko Nishigami[a,d], Yoji Osako[b,d], Kenjiro Tanaka[b], Kazunari Yuri[b], Motohiro Kawasaki[c,d], Tatsunori Ikemoto[c,d], Matthew McLaughlin[d], Kenji Ishida[a], Toshikazu Tani[c], Takahiro Ushida[c,d,e,*]

[a] Rehabilitation Center, Kochi Medical School Hospital, Nankoku, Japan
[b] Department of Neurobiology & Anatomy, Kochi Medical School, Nankoku, Japan
[c] Department of Orthopaedic Surgery, Kochi Medical School, Nankoku, Japan
[d] Nankoku Pain Research Group, Kochi Medical School, Kochi, Japan
[e] Multidisciplinary Pain Center, Aichi Medical University, 21 Karimata, Yazako, Nagakute, Aichi 480-1195, Japan

ARTICLE INFO

Article history:
Received 18 November 2008
Received in revised form 28 January 2009
Accepted 7 February 2009

Keywords:
Long-term joint immobilization
Pain
Calcitonin gene-related peptide
Dorsal root ganglion
Spinal dorsal horn
Posterior nuclei

ABSTRACT

Long-term immobilization by casting can occasionally cause pathologic pain states in the immobilized side. The underlying neurophysiological mechanisms of immobilization-related pain are not well understood. For this reason, we specifically examined changes of calcitonin gene-related peptide (CGRP) expression in the dorsal root ganglion (DRG), spinal dorsal horn and posterior nuclei (cuneate nuclei) in a long-term immobilization model following casting for 5 weeks. A plastic cast was wrapped around the right limb from the forearm to the forepaw to keep wrist joint at 90° of flexion. In this model, CGRP in immobilized (ipsilateral) side was distributed in larger DRG neurons compared with contralateral side, even though the number of CGRP-immunoreactive (CGRP-IR) neurons did not differ. Spinal laminae III–V, not laminae I–II in ipsilateral side showed significantly high CGRP expression relative to contralateral side. CGRP expression in cuneate nuclei was not significantly different between ipsilateral and contralateral sides. Long-term immobilization by casting may induce phenotypic changes in CGRP expression both in DRG and spinal deep layers, and these changes are partly responsible for pathological pain states in immobilized side.

Casting (immobilization) is commonly utilized because it is considered to be useful in restoring injured organs by local resting. However, long-term immobilization results in harmful complications such as muscular atrophy or joint contracture in the immobilized side. In addition, recent research reveals that immobilization may cause not only motor dysfunction but also sensory-motor or autonomic nerve dysfunction, and occasionally immobilization-related pain [5,19,26]. With regard to immobilization-related neurological dysfunction, Butler et al. reported observing signs of neglect-like states and complex regional pain syndromes after casting limbs of patients with foot fractures and healthy volunteers [2]. Therefore, long-term immobilization may limit therapeutic outcome and may produce low levels of activity of daily living.

Predominantly, immobilization-related pain has been considered to be a result of shortened muscle and the adhesion of joints and periarticular structures. Clinically, surgical release of the periarticular tissues has been successful in helping relieve patients with painful post-traumatic contracture [3]. Previously, we developed a long-term joint immobilization model, which showed a joint contracture, disuse tendencies, and pain behaviors in the affected limb, and we observed changes in electrophysiological responses of dorsal horn neurons to mechanical stimuli and motion stimuli [27]. This observation suggests that central changes as well as local peripheral changes are implicated in immobilization-related pain. It is well known that intense nociceptive stimulation (e.g., inflammation, nerve injury and cancer) alters the character of neurons in the central nervous system [1,7,28] and these alterations are considered to be the cause of allodynia and hyperalgesia [22,24]. However, it remains unclear how these central neuronal changes occur under conditions of sensory input deprivation (long-term immobilization).

In the present study, we have focused on the expression of calcitonin gene-related peptide (CGRP). CGRP has a wide distribution throughout the central and peripheral systems and is involved in processing nociceptive information. Firstly, in the spinal cord, CGRP is released from C and Aδ nociceptive afferent fibers as an excitatory neurotransmitter and neuromodulator following painful stimuli, and sensitizes dorsal horn neurons [6,20]. In the experimental animals showing mechanical allodynia and hyperalgesia, CGRP

* Corresponding author. Tel.: +81 561 62 5004; fax: +81 561 62 5004.
E-mail address: ushidat-koc@umin.ac.jp (T. Ushida).

0304-3940/$ – see front matter © 2009 Elsevier Ireland Ltd. All rights reserved.
doi:10.1016/j.neulet.2009.02.043

expression in the spinal dorsal horn was markedly up-regulated [9,15]. Secondly, changes in CGRP expression within the dorsal root ganglion (DRG) have been studied in various pain models. The number of CGRP-immunoreactive (CGRP-IR) DRG neurons increased or decreased in inflammatory and neuropathic pain models [11,14,21]. In these studies, phenotypic changes in DRG CGRP expression have included both a change in the number of CGRP-IR neurons and a switch to CGRP expression in small or large DRG neurons. Interestingly, in neuropathic pain models, CGRP expression in the posterior nuclei (where information is conveyed by thick myelinated fibers encoding tactile sensation relayed to higher levels) significantly increased in the injured side, suggesting that CGRP released in non-nociceptive pathways is implicated in pain states [11,12]. The aim of the present study was to examine whether the expression of CGRP in DRGs, spinal dorsal horn, and posterior nuclei (cuneate nuclei) altered under conditions of long-term immobilization, to gain a better understanding of immobilization-related pain.

All animal experiments were approved by the Kochi Medical School Animal Care and Use Committee and were performed at Kochi Medical School. Seven adult male Sprague–Dawley rats (250–300 g; Japan SLC, Inc.) were used in this study. Long-term joint immobilization was maintained by using a plastic cast as described previously [27]. Briefly, the rats were anesthetized with tribromoethanol (200 mg/kg i.p.), and a plastic cast was wrapped around the right limb from the forearm to the forepaw to keep wrist joint at 90° of flexion. After 5 weeks casting, the rats were perfused transcardially with 4% paraformaldehyde and DRGs, spinal cord, and medulla oblongata were excised at 24 h after removing cast. Retrograde fluorogold labeling demonstrated that DRG neurons innervating the wrist joint in the rat were distributed throughout DRGs from C6 to Th1 levels, and most of the labeled neurons contained CGRP [8]. Hence, DRGs and spinal cords from C7 to Th1 levels were harvested and used for CGRP immunohistochemistry. All of the sections were cut on a cryostat at a thickness of 12 μm (in DRG) and 23 μm (in spinal cord and medulla oblongata), and were incubated in the primary antibody to CGRP (1:5000, Sigma) for 48 h at 4 °C and antibody labeling was detected using Alexa Fluor 488 (1:1000, Molecular Probes). For size distributions of the CGRP-IR neuronal profile, the areas of over 2000 DRG neurons were measured in each side, on both the immobilized (ipsilateral) and contralateral sides, using imaging analysis software (NIH Image). To calculate the number of CGRP-IR neurons, one hundred fluorescent images of ipsilateral and contralateral DRGs were extracted per animal at random (700 fluorescent images total each side), and the number of CGRP-IR neurons was counted. Only CGRP-IR neurons with visible nuclei were selected for measurement. The total area of CGRP fibers (pixels) in superficial layers (laminae I–II) and deep layers (laminae III–V) in spinal dorsal horn and posterior nuclei (cuneate nuclei) in medulla oblongata was quantitatively evaluated using NIH Image. The differences in the number of CGRP-IR neurons and total area of CGRP fibers between the ipsilateral and contralateral sides were assessed using unpaired *t*-tests. The differences in size distribution of DRG neurons were assessed using Kolmogorov–Smirnov test. Statistically significant differences between groups were expressed as *p*-values less than 0.05.

No significant differences in the number of CGRP-IR DRG neurons were found between ipsilateral (282.7 ± 33.5) and contralateral sides (279.5 ± 33.7). However, the size distribution of ipsilateral CGRP-IR DRG neurons was significantly different from that of the contralateral side ($p < 0.0001$, Fig. 1); ipsilateral CGRP expression was observed in larger neurons on the contralateral side. The size distributions of Nissl-stained DRG neurons were no different in the ipsilateral and contralateral sides ($p = 0.228$), demonstrating that all ipsilateral DRG neurons did not become larger, independent of CGRP expression.

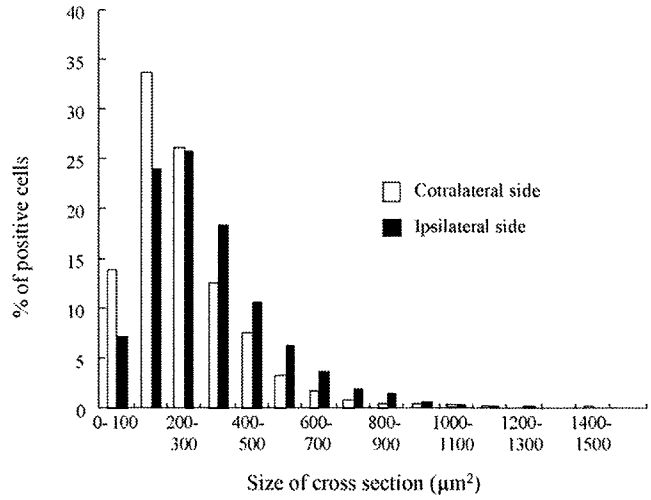

Fig. 1. Size distribution analysis of CGRP-IR in DRG neurons after joint immobilization. There were shifts toward larger cell sizes in the size distribution of CGRP-IR of immobilized (ipsilateral) side in DRG neurons (Kolmogorov–Smirnov test: $p < 0.0001$).

In the spinal cord, the areas of ipsilateral CGRP-IR fibers significantly increased compared with the contralateral side in laminae III–V (ipsilateral, 460,028 ± 89,537 pixels; contralateral, 365,932 ± 67,834 pixels: $p < 0.05$) but not in laminae I–II (ipsilateral, 642,202 ± 78,683 pixels; contralateral, 620,055 ± 65,095 pixels: NS, Fig. 2). No significant change was observed in cuneate nuclei CGRP-IR fibers between the ipsilateral (33,810 ± 17,762 pixels) and contralateral sides (28,683 ± 13,514 pixels).

The present study revealed that long-term immobilization by casting induced an up-regulation of CGRP expression, not in superficial but in deep layers of dorsal horn and a shift in the distribution of CGRP expression profile to larger DRG neurons. When classifying DRG neurons in terms of size, CGRP production is known to be observed not only in small to medium neurons, but also in large DRG neurons. According to previous studies, the majority of small neurons have C fiber axons, which project to the superficial layers of the spinal dorsal horn. In contrast, the large neurons correspond to Aα or Aβ fibers, which project to the deep layers of the spinal dorsal horn or posterior nuclei. Previous studies demonstrated that there were shifts toward larger cell sizes in the size distribution of CGRP-IR DRG neurons and further CGRP expression in posterior nuclei increased in neuropathic pain models [11,12]. In addition, spontaneous activity and excitability of posterior nuclei in the nerve injury side were significantly higher than in the contralateral side [13]. Although these observations suggest that an up-regulation of posterior nuclei plays an important role in the generation and maintenance of pain, CGRP expression in posterior nuclei was not significantly affected by long-term immobilization in the present study. As evidenced by a retrograde tracing study, CGRP-IR fibers from medium-size lumbar DRG neurons project to posterior nuclei [16,25], but the projection of those from cervical DRG neurons is still unknown. Further research is needed to clarify which size cervical DRG neurons are the ones which predominantly project to posterior nuclei.

In a previous report, endoneurial injection of nerve growth factor (NGF) increased the percentage of large-sized CGRP-IR DRG neurons [18]. Therefore, NGF seems to be implicated in a switch to CGRP expression in larger DRG neurons. However, the detailed mechanism of CGRP expression in the DRG, regulated by NGF, remains unknown. NGF also is induced by Schwann cells after nerve injury and is involved in the onset of pain behaviors in neuropathic pain [10,17]. In the current joint immobilization model,

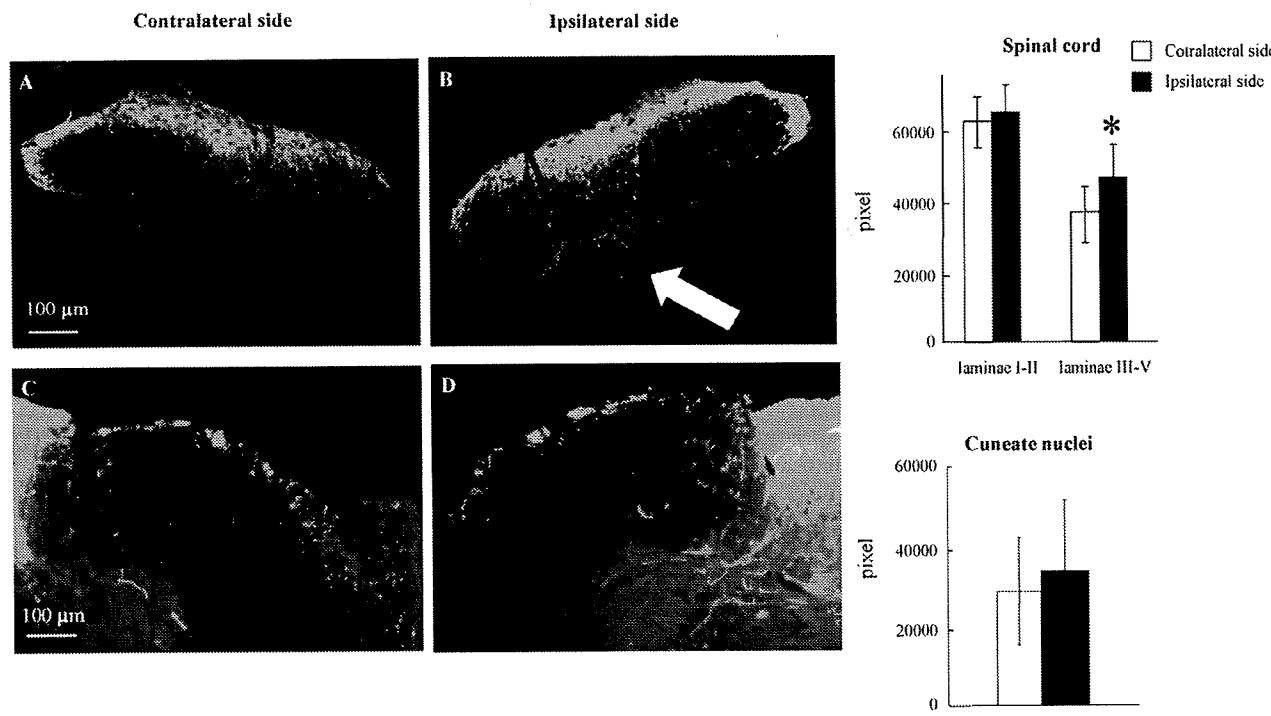

Fig. 2. Photomicrographs and histogram of CGRP-IR fibers in spinal dorsal horn (A and B) and cuneate nuclei (C and D) after joint immobilization. The results of histogram are expressed as means ± S.E.M. of pixel. CGRP-IR fibers in laminae I–II and cuneate nuclei were not significantly different between immobilized (ipsilateral) side and contralateral side. However CGRP-IR fibers significantly increased in laminae III–V of ipsilateral side (B, arrow) compared with contralateral side. $^{*}p < 0.05$.

peripheral nerves might be injured by long-term casting. Having said that, there was no evidence of peripheral nerve injury or NGF up-regulation after joint immobilization.

In the deep layers, where CGRP expression was up-regulated by long-term immobilization, there was a distribution of wide-dynamic range (WDR) neurons. The WDR neurons have been proven to respond to both noxious and innocuous stimuli in electrophysiological studies. Growing evidence suggests that neuronal discharge of WDR neurons is involved in pathological pain conditions, such as allodynia and hyperalgesia. Allodynic rats showed a significant decrease in the proportion of low-threshold neurons and an increase in the proportion of WDR neurons [4]. Electrophysiological recording from WDR neurons in the spinal dorsal horn in hyperalgesic rats significantly increased spontaneous activity and after-discharges to noxious mechanical stimuli [29]. Furthermore, the administration of CGRP8-37, a selective CGRP receptor antagonist, induced a significant decrease in the evoked discharge frequency of WDR neurons [23]. Therefore, the up-regulation of CGRP expression in the spinal deep layers might modulate nociception through WDR neuronal activation in the present immobilization model. Indeed, we have previously demonstrated that the population of WDR neurons in the immobilized side increased after joint immobilization [27].

In conclusion, long-term casting induces the phenotypic changes in CGRP expression both at the DRG and spinal cord levels (specifically in deep layers) on the immobilized side. In terms of pathological pain states after long-term joint immobilization, these alterations may be of extreme importance.

References

[1] S. Balasubramanyan, P.L. Stemkowski, M.J. Stebbing, P.A. Smith, Sciatic chronic constriction injury produces cell-type-specific changes in the electrophysiological properties of rat substantia gelatinosa neurons, J. Neurophysiol. 96 (2006) 579–590.
[2] S.H. Butler, M. Nyman, T. Gordth, Immobility in volunteers produces signs and symptoms of CRPS (1) and a neglect-like state, in: 9th World Congress on Pain, vol. 52, IASP Press, Seattle, 1999 (Abstracts).
[3] M.S. Cohen, H. Hastings, Post-traumatic contracture of the elbow. Operative release using a lateral collateral ligament sparing approach, J. Bone Joint Surg. Br. 80 (1998) 805–812.
[4] J.X. Hao, R.C. Kupers, X.J. Xu, Response characteristics of spinal cord dorsal horn neurons in chronic allodynic rats after spinal cord injury, J. Neurophysiol. 92 (2004) 1391–1399.
[5] F. Kaneko, T. Murakami, K. Onari, H. Kurumadani, K. Kawaguchi, Decreased cortical excitability during motor imagery after disuse of an upper limb in humans, Clin. Neurophysiol. 114 (2003) 2397–2403.
[6] I. Kangrga, M. Randic, Tachykinins and calcitonin gene-related peptide enhance release of endogenous glutamate and aspartate from the rat spinal dorsal horn slice, J. Neurosci. 10 (1990) 2026–2038.
[7] S.G. Khasabov, D.T. Hamamoto, C. Harding-Rose, D.A. Simone, Tumor-evoked hyperalgesia and sensitization of nociceptive dorsal horn neurons in a murine model of cancer pain, Brain Res. 1180 (2007) 7–19.
[8] K. Kuniyoshi, S. Ohtori, N. Ochiai, R. Murata, T. Matsudo, T. Yamada, S.S. Ochiai, H. Moriya, K. Takahashi, Characteristics of sensory DRG neurons innervating the wrist joint in rats, Eur. J. Pain 11 (2007) 323–328.
[9] S.E. Lee, J.H. Kim, Involvement of substance P and calcitonin gene-related peptide in development and maintenance of neuropathic pain from spinal nerve injury model of rat, Neurosci. Res. 58 (2007) 245–249.
[10] L. Li, C.J. Xian, J.H. Zhong, X.F. Zhou, Lumbar 5 ventral root transection-induced up-regulation of nerve growth factor in sensory neurons and their target tissues: a mechanism in neuropathic pain, Mol. Cell. Neurosci. 23 (2003) 232–250.
[11] W. Ma, M.A. Bisby, Increase of calcitonin gene-related peptide immunoreactivity in the axonal fibers of the gracile nuclei of adult and aged rats after complete and partial sciatic nerve injuries, Exp. Neurol. 152 (1998) 137–149.
[12] K. Miki, T. Fukuoka, A. Tokunaga, K. Noguchi, Calcitonin gene-related peptide increase in the rat spinal dorsal horn and dorsal column nucleus following peripheral nerve injury: up-regulation in a subpopulation of primary afferent sensory neurons, Neuroscience 82 (1998) 1243–1252.
[13] K. Miki, K. Iwata, Y. Tsuboi, R. Sumino, T. Fukuoka, T. Tachibana, A. Tokunaga, K. Noguchi, Responses of dorsal column nuclei neurons in rats with experimental mononeuropathy, Pain 76 (1998) 407–415.
[14] S. Ohtori, K. Takahashi, T. Chiba, M. Yamagata, H. Sameda, H. Moriya, Phenotypic inflammation switch in rats shown by calcitonin gene-related peptide immunoreactive dorsal root ganglion neurons innervating the lumbar facet joints, Spine 26 (2001) 1009–1013.
[15] R. Oku, M. Satoh, N. Fujii, A. Otaka, H. Yajima, H. Takagi, Calcitonin gene-related peptide promotes mechanical nociception by potentiating release of substance P from the spinal dorsal horn in rats, Brain Res. 403 (1987) 350–354.

[16] J.K. Persson, B. Lindh, R. Elde, B. Robertson, C. Rivero-Melián, N.P. Eriksson, T. Hökfelt, H. Aldskogius, The expression of different cytochemical markers in normal and axotomised dorsal root ganglion cells projecting to the nucleus gracilis in the adult rat, Exp. Brain Res. 105 (1995) 331–344.
[17] M.S. Ramer, M.A. Bisby, Adrenergic innervation of rat sensory ganglia following proximal or distal painful sciatic neuropathy: distinct mechanisms revealed by anti-NGF treatment, Eur. J. Neurosci. 11 (1999) 837–846.
[18] G. Ruiz, J.E. Baños, The effect of endoneurial nerve growth factor on calcitonin gene-related peptide expression in primary sensory neurons, Brain Res. 1042 (2005) 44–52.
[19] M. Shibata, K. Abe, A. Jimbo, T. Shimizu, M. Mihara, S. Sadahiro, H. Yoshikawa, T. Mashimo, Complex regional pain syndrome type I associated with amyotrophic lateral sclerosis, Clin. J. Pain 19 (2003) 69–70.
[20] D.H. Smullin, S.R. Skilling, A.A. Larson, Interactions between substance P, calcitonin gene-related peptide, taurine and excitatory amino acids in the spinal cord, Pain 42 (1990) 93–101.
[21] P.C. Staton, A.W. Wilson, C. Bountra, I.P. Chessell, N.C. Day, Changes in dorsal root ganglion CGRP expression in a chronic inflammatory model of the rat knee joint: differential modulation by rofecoxib and paracetamol, Eur. J. Pain 11 (2007) 283–289.
[22] H. Sun, K. Ren, C.M. Zhong, M.H. Ossipov, T.P. Malan Jr., J. Lai, F. Porreca, Nerve injury-induced tactile allodynia is mediated via ascending spinal dorsal column projections, Pain 90 (2001) 105–111.
[23] R.Q. Sun, N.B. Lawand, Q. Lin, W.D. Willis, Role of calcitonin gene-related peptide in the sensitization of dorsal horn neurons to mechanical stimulation after intradermal injection of capsaicin, J. Neurophysiol. 92 (2004) 320–326.
[24] R.Q. Sun, N.B. Lawand, W.D. Willis, The role of calcitonin gene-related peptide (CGRP) in the generation and maintenance of mechanical allodynia and hyperalgesia in rats after intradermal injection of capsaicin, Pain 104 (2003) 201–208.
[25] M. Tamatani, E. Senba, M. Tohyama, Calcitonin gene-related peptide- and substance P-containing primary afferent fibers in the dorsal column of the rat, Brain Res. 495 (1989) 122–130.
[26] A.J. Terkelsen, F.W. Bach, T.S. Jensen, Experimental forearm immobilization in humans induces cold and mechanical hyperalgesia, Anesthesiology 109 (2008) 297–307.
[27] T. Ushida, W.D. Wills, Changes in dorsal horn neuronal responses in an experimental wrist contracture model, J. Orthop. Sci. 6 (2001) 46–52.
[28] K.S. Vikman, A.W. Duggan, P.J. Siddall, Increased ability to induce long-term potentiation of spinal dorsal horn neurones in monoarthritic rats, Brain Res. 990 (2003) 51–57.
[29] H.R. Weng, J.V. Cordella, P.M. Dougherty, Changes in sensory processing in the spinal dorsal horn accompany vincristine-induced hyperalgesia and allodynia, Pain 103 (2003) 131–138.

SPINE Volume 34, Number 2, pp E83–E87

Use of the Finite Element Method to Study the Mechanism of Spinal Cord Injury Without Radiological Abnormality in the Cervical Spine

Yasuaki Imajo, MD, Isamu Hiiragi, Yoshihiko Kato, and Toshihiko Taguchi

Study Design. Three-dimensional C3–C5 and C3–C4 finite element (FE) models were used to analyze biomechanical responses under compression and extension moments.

Objective. To validate our models against other published FE models and experimental studies and improve our understanding of the mechanism of spinal cord injury without radiologic abnormality (SCIWORA) in cervical spine.

Summary of Background Data. The underlying mechanism for SCIWORA remains unclear. We hypothesized that the incidence of SCIWORA was associated with facet joint morphology and bony pincers mechanism.

Methods. FE models were constructed using data from computed tomography scans of the cervical spine of a healthy young man. The C3–C5 FE models consisted of bony vertebra, articulating facets, and intervertebral disc. Facet surfaces were oriented at 30°, 45°, and 60° from the transverse plane. These models were constrained in all degrees of freedom at the C5 inferior vertebral body and a uniform axial displacement of 1 mm was applied to the superior nodes of C3. Three model versions changed to C3–C4 models with ligaments. The C4 inferior-most bony nodes were constrained, whereas the top of the C3 superior-most bony nodes were left unconstrained. These models were subjected to an axial compression load of 73.6 N with extension moments (1.8 Nm) applied to the upper bony section C3 vertebra. The predicted responses were compared with published results.

Results. The response under axial compression was validated and corresponded closely with published results. Under sagittal moment, the C3–C4 FE model with 60° facet was the most flexible in extension (4.22°). Total translation was highest for the model with 60° facet.

Conclusion. The load displacement response of C3–C5 FE models was in agreement with published data. We confirmed that the C3–C4 FE model with 60° facet was the most susceptible to SCIWORA and that the bony pincers mechanism was dependent on facet joint inclination.

Key words: cervical spine, finite element methods, spinal cord injury without radiologic abnormality, bony pincers mechanism. **Spine 2009;34:E83–E87**

Since the first description by Pang and Wilberger, spinal cord injuries without radiologic abnormality (SCIWORA) have been well documented in the pediatric literature.[1–4] The cervical spine (C3–C4) is the most frequent site of SCIWORA in the spinal column.[5,6] Many studies have been conducted in an attempt to understand the mechanism underlying SCIWORA, however, this remains unclear. We hypothesized that SCIWORA was associated with facet joint morphology at C3–C4. The finite element (FE) method of analysis is one of the most popular approaches used to study the biomechanics of the cervical spine. We made 3 detailed FE models of C3–C5 with different facet joint morphology closely akin to the human cervical spine. With the aim of better understanding the underlying mechanism of SCIWORA, we investigated the properties of these models in comparison to other FE models and to an *in vitro* experimental study.

Materials and Methods

Structural geometry and material properties are very important for accurate analysis of the biomechanical response of motion segments. To prepare a three-dimensional FE model, C3–C5 motion segment data were obtained from computed tomography scans (2-mm intervals; TCT-900S, Toshiba, Tokyo, Japan) of the cervical spine of a 29-year-old man with no abnormal findings on roentgenograms. A solid model for the C3–C5 cervical spine structure was developed according to the principles of three-dimensional reconstruction. A three-dimensional, 8-noded solid element was used for meshing the cortical bone, cancellous bone, endplate, posterior arch, intervertebral disc annulus, and nucleus. The Link element (LINK10) was used for ligaments and capsular ligaments. Link[7] is a three-dimensional spar element having the unique feature of a bilinear stiffness matrix resulting in a uniaxial tension-only (or compression-only) element. In our models, facet articulation was treated as a moving contact problem, defined contact elements to models the changing areas of contact of facet articulating surfaces with increments in loading. The Contact element (CONTA173) was used for the facet joints. Material properties for each element type were obtained from the literature (Table 1).[7–11] The FE model of the 3 vertebra segment C3–C5 U consisted of 23,192 elements, and 7786 nodes that modeled the bony vertebra, articulating facets, and intervertebral disc (Figure 1). The intervertebral disc was represented as a continuum structure occupying the intervertebral space. Each intervertebral disc consisted of a disc annulus, disc nucleus, and endplates. The assumed anterior and posterior disc heights were 5.5 and 3.5 mm, respectively. These correspond to mean values reported in the literature for a healthy cervical intervertebral disc.[8] Also modeled were the anterior longitudinal ligament (ALL), the posterior longitudinal ligament (PLL), the ligamentum flavum (LF), the interspinous ligament (ISL), the supraspinous ligament (SSL), and the capsular ligament (CL). All ligaments were modeled as continua and included contact elements in the facet

From the Department of Orthopaedic Surgery, Yamaguchi University Graduate School of Medicine, Yamaguchi, Japan.
Acknowledgment date: January 21, 2008. Revision date: July 21, 2008. Acceptance date: July 25, 2008.
The manuscript submitted does not contain information about medical device(s)/drug(s).
No funds were received in support of this work. No benefits in any form have been or will be received from a commercial party related directly or indirectly to the subject of this manuscript.
Address correspondence and reprint requests to Yasuaki Imajo, MD, Department of Orthopaedic Surgery, Yamaguchi University Graduate School of Medicine 1-1 Minami-kogushi, Ube, Yamaguchi, 755-8505, Japan; E-mail: i-yasuak@yamaguchi-u.ac.jp

Table 1. Material Properties Used in the Present Study

Material	Young's Modulus (MPa)/Poisson's Ratio				
	Maurel *et al*[7]	Goel and Clausen[9]	Kumaresan *et al*[8]	Teo and Ng[10]	Our Models
Cortical bone	12000/0.3	10000/0.3	10000/0.29	10000/0.29	10000/0.29
Cancellous bone	100/0.2	450/0.25	100/0.29	100/0.29	100/0.29
Endplate	300/0.3	2000/0.20	500/0.40	500/0.40	500/0.40
Posterior elements	6000/0.3	3500/0.25	3500/0.29	3500/0.29	3500/0.29
Disc annulus	2.5/0.45	4.2/0.45	3.4/0.40	3.4/0.40	3.4/0.40
Disc nucleus	—	—	3.4/0.49	1.0/0.499	1.0/0.499
ALL	10/-	15–30/0.30	54.5/0.39	54.5/-	54.5/0.30
PLL	20/-	10–20/0.30	30/0.39	20/-	20/0.30
LF	50/-	5.0–10.0/0.30	1.5/0.39	1.5/-	1.5/0.30
ISL	3/-	4.0–8.0/0.30	1.5/0.39	1.5/-	1.5/0.30
SSL	3/-	4.0–8.0/0.30	1.5/0.39	1.5/-	1.5/0.30
CL	20/-	7–30/0.30	2/0.39	20/-	20/0.30

ALL indicates anterior longitudinal ligament; PLL, posterior longitudinal ligament; LF, ligamentum flavum; ISL: intraspinous ligament; SSL, supraspinous ligament; CL, capsular ligament.

joints. Three models were developed with 3 versions of facet joint inclination. Facet surfaces were oriented at 30°, 45°, and 60° from the transverse plane. These FE models of the intact C3–C5 spine unit were healthy segments without any degenerative signs. The C3–C5 models were constrained in all degrees of freedom at the C5 inferior vertebral body. A uniform axial displacement of 1 mm was applied incrementally in 5 steps to the superior nodes of C3. To evaluate the force-displacement response against other FE models and experimental measurements *in vitro*, FE method analysis about deformation behavior of cervical spine (C3–C5) was performed using above FE models and a commercially available finite-element modeling software (ANSYS, Canonsburg, PA). The above FE models were used to compare the force-displacement response with other FE models and with *in vitro* experimental measurements. Three model versions changed to C3–C4 models. These C4 inferior-most bony nodes were constrained, whereas the top of the C3 superior-most bony nodes were left unconstrained. The models were subjected to an axial compression load (preload) of 73.6 N with extension moments (1.8 Nm) applied to the upper bony section C3 vertebra. The predicted responses were validated against *in vitro* experimental results and analytical results.

The analysis is based on the assumption that vertebra bodies are rigid and do not deform. A maximum extension moment of 1.8 Nm was approximately 20% of the failure load of 10 Nm.[12]

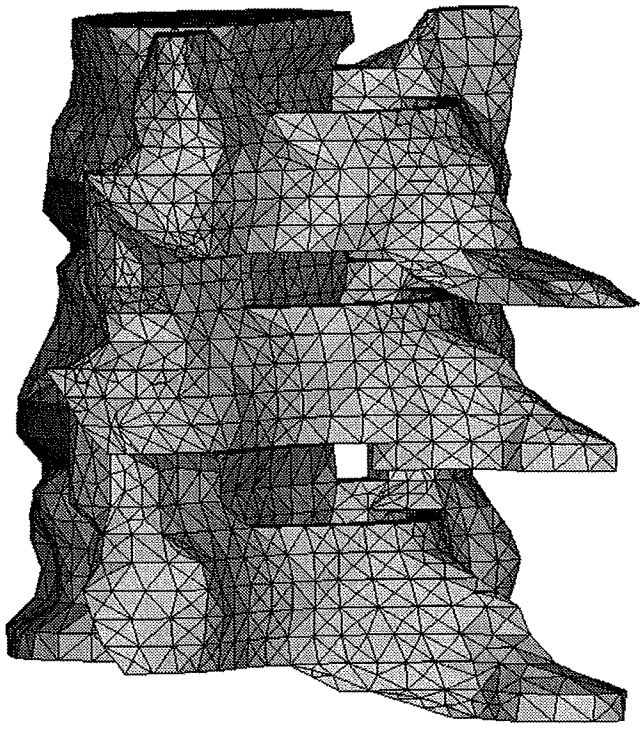

Figure 1. C3–C5 FE model with 45° facet.

■ Results

It seemed reasonable to suppose that the response to axial compression was nonlinear. The biomechanical response of these models was validated and corresponded closely with the results of experimental measurements made *in vitro* (Figure 2A) and with existing analytical models (Figure 2B). In particular, the 30° facet of our models was in very close agreement with experimental measurements. Table 2 shows the comparison of results between our C3–C4 models, experimental data, and analytical models under an axial compression load (preload) of 73.6 N with extension moments of 1.8 Nm. Because the present models were assumed to be symmetrical about the midsagittal plane, no coupled motion was predicted for the extension load configurations. The 45° facet of our models was in good agreement with mean experiment data. The C3–C4 FE model with a 60° facet was the most flexible in the extension motion. The inferior articular facet of C3 was contacted the superior articular facet of C4 and slided on the surface of the superior articular facets of C4 in our all models under an axial compression load (preload) of 73.6 N with extension moments of 1.8 Nm. However, facet deformation was confirmed. Table 3 shows posterior and inferior translation of the infra-posterior edge of C3 vertebra. Total translation comprised both posterior and inferior translation. Total and inferior translation was highest for the C3–C4 FE model with 60° facet, whereas posterior translation was highest for the C3–C4 FE model with 30° facet. Table 4 shows the distance from the posteroinferior margin of the C3 vertebral body to the anterosuperior margin of the C4 lamina in the extension

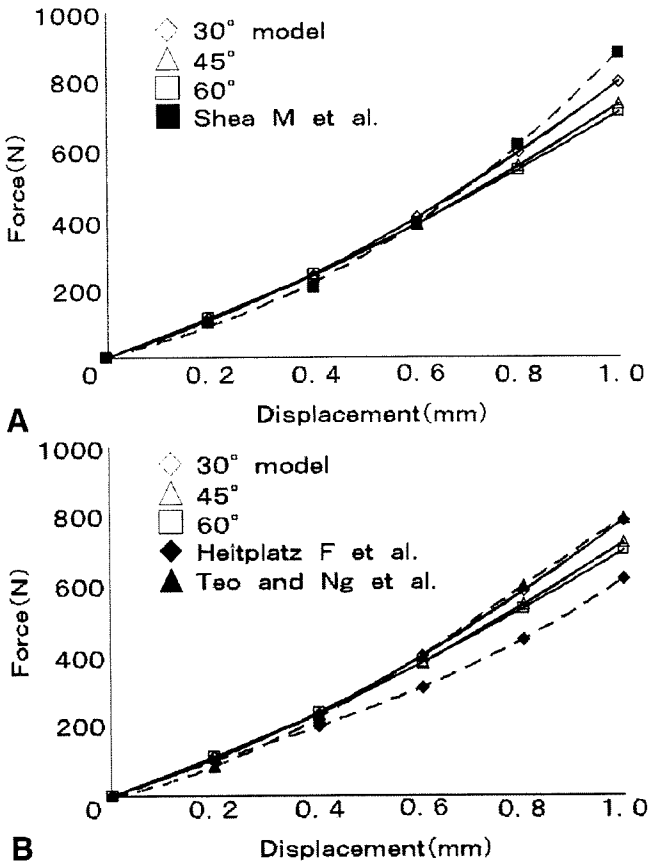

Figure 2. **A,** Comparison of results from the present C3–C5 FE models with 30°, 45°, and 60° facets against experimental values published by Shea *et al.* **B,** Comparison of results from the present FE models with analytical results by Teo and Ng and Heitplatz *et al.*

motion. The C3–C4 FE model with 60° facet was the shortest distance.

■ Discussion

SCIWORA is defined as the occurrence of acute traumatic myelopathy despite normal findings with plain radiographs and computed tomography. Ueta reported 147 patients with SCIWORA of the cervical spine. The injury site was at a single level only in 130/147 (88%) patients, affecting the C3–C4 intervertebral level in 99 (67%) patients.[5] Kawai and Yabuno reported 60 patients with SCIWORA of the cervical spine.[6] Of these, 30 (50%) sustained SCIWORA at C3–C4. Several workers have investigated the pathology of SCIWORA in the cervical spine; however, this remains largely unknown. Taylor and Blackwood reported that injuries causing cervical cord damage in the absence of vertebral fracture or dislocation were usually sustained by forcible extension of the neck rather than by hyperflexion.[13] In 1951, Taylor suggested that when cord compression occurred and no fracture of the vertebral column or rupture of its ligaments could be discerned, a rational explanation for cord damage was forward bulging of the ligamentum flavum between C3 and C4 levels during extreme hyperextension.[14] In chronic myelopathy, Penning reported that the bony pincers mechanism must be at least as important as the mechanism of bulging of soft ligamentum flavum.[15] In the bony pincers mechanism, the cervical spinal cord in extension is compressed between bony pincers formed by the anterior aspect of the arch of the inferior vertebra on 1 side and the posterior-inferior aspect of the bony part of the superior vertebra on the other (Figure 3). We hypothesized that the cause of SCIWORA was associated with the bony pincers mechanism and investigated this possible mechanism using our FE models.

Table 3. Translation of Infraposterior Edge of C3 Vertebra in Extension

Our Models	Posterior Translation	Inferior Translation	Total Translation
30°	0.41	0.37	0.55
45°	0.40	0.43	0.59
60°	0.36	0.54	0.65

The extension moment was affected by the facet joints. During extension, the superior facet surfaces slid down and backwards relative the inferior facet and the posterior region of the facet joint was compressed. The facet joint gap also underwent a narrowing during extension. Pearson *et al* reported that facet joint kinematics were evaluated during simulated whiplash of whole cervical spine specimens with muscle force replication[16]. They confirmed facet joint compression (displacement of the superior facet surface towards the inferior facet surface) and facet joint sliding (displacement of the superior facet surface along the lower facet surface) in the lower cervical spine. Kaneoka *et al* reported that the C5–C6 intervertebral center of rotation was dynamically shifted superiorly during simulated whiplash impacts, implying that facet articular surfaces were forcefully compressed during intervertebral extension in an *in vivo* study.[17] Since a maximum extension moment of 1.8 Nm was small moment compared with other studies and our models were not subjected to shear moment backwards.

Table 2. Predicted Rotations Compared With Present Models, Published Experimental Data, and Analytical Models

	Rotation(°)						
	Experimental		Finite Element Models		Our Models		
73.6 N Preload	Moroney *et al*	Pelker *et al*	Goel *et al*	Teo *et al*	30°	45°	60°
At 1.8Nm extension moment Extention	3.52	3.45	3.69	3.95	3.16	3.47	4.22

Table 4. The Distance From the Posteroinferior Margin of the C3 Vertebral Body to the Anterosuperior Margin of the C4 Lamina in Extension

Our Models	
30°	13.00 mm
45°	12.97 mm
60°	12.93 mm

Many studies have investigated the mechanical response of the human cervical spine under physiologic loads. FE analysis has been applied successfully in the field of biomechanics. This method offers the advantages of being able to handle complex geometric configurations and material and geometric nonlinearity. Validation is the most important step during FE analysis of anatomic structure modeling and the use of FE models beyond their validated conditions is a common error. Model validation allows an analytical model to produce reliable predictions for a variety of complex investigations. In this study, the loads and constraints of the validation step for extension and axial compressive load configurations were identical to the published literature. The loads applied to the C3–C5 analysis models corresponded to the experimental values used in studies carried out by Shea *et al.*[18] For the applied compressive displacement at C3, the predicted vertical reaction at C5 (*i.e.*, the force transmitted to C5) was compared to published results.[7,11,18,19] For the applied moment at C3, rotational responses of C3 with respect to C4 in the plane of moment application were computed and compared with published results.[7,10,12,20]

Force-displacement of the human cervical spine is recognized as being nonlinear, with increasing stiffness at higher loads.[7,8,10,11,19,21,22] It is important to develop realistic FE models that effectively simulate this nonlinear behavior of the human cervical spine. The C3–C5 FE models used in the present study could predict the biomechanical response of the human cervical spine under an axial compressive displacement of up to 1 mm and were validated against published data.

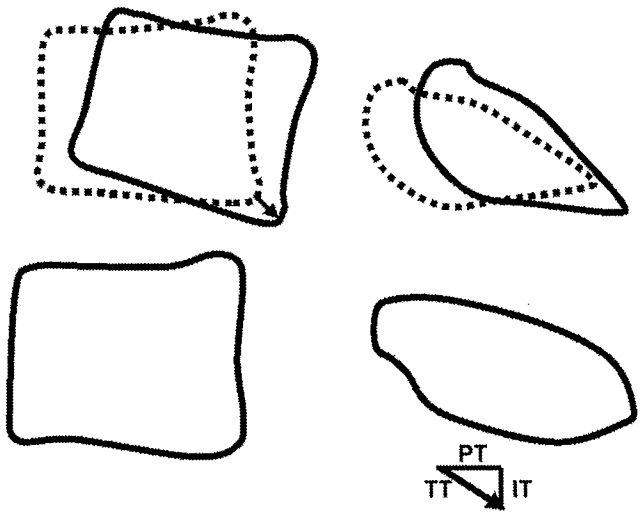

Figure 3. Narrowing of the spinal canal in extension, caused by a bony pincer mechanism acting between the body of C3 vertebra and the arch of C4 vertebra. TT indicates total translation (arrow); IT, inferior translation; PT, posterior translation.

Under sagittal moment, the C3–C4 FE model with 60° facet was the most flexible in extension (4.22°) at 1.8-Nm moment. The predicted rotation was 3.47° and 3.16° at 1.8 Nm extension for the C3–C4 FE model with 45° and 30° facet, respectively. The predicted rotation for our C3–C4 models agrees with computed results published by Moroney *et al*, Pelker *et al*, Goel *et al*, and Teo *et al.*[7,10,12,20] In particular, the C3–C4 FE model with 45° facet correlated well with experimental data by Pelker *et al* and Moroney *et al.*[12,20] Panjabi *et al* reported that the inclination of the superior articular facet in relation to the transverse plane was 48.8° at C3, 47.0° at C4, and 45.8° at C5.[23] The FE model with 45° facet most closely resembled the facet joint morphology of the human cervical spine. Under extension moment, total translation was highest for the C3–C4 FE model with 60° facet. The distance between bony pincers formed by the anterior aspect of the arch of C4 vertebra and the posterior-inferior aspect of the bony C3 vertebra was shortest for the C3–C4 FE model with 60° facet. Therefore, we confirmed the bony pincers mechanism was dependent on facet joint inclination. In this study, we could not account for cervical spinal cord damage *via* infolding of the ligamentum flavum. However, we could explain the damage by invoking the bony pincers mechanism suggested by Penning.[15] Ueta reported that the cause of SCIWORA involves the anatomy of the human cervical spine.[5]

Muscle tension in neck may affect the causes of SCIWORA. However, our models did not include muscles (active or passive effects) or overlaying soft tissue. It was because the biggest obstacle in the human cervical spine modeling was the lack of experimental data for this region of the spine.

We confirmed here that an increase in facet joint inclination is one of the causes of SCIWORA.

■ Key Point

• Three-dimensional C3–C5 and C3–C4 finite element models were used to analyze biomechanical responses under compression and extension moments. We hypothesized that the incidence of spinal cord injury without radiologic abnormality was associated with facet joint morphology and bony pincers mechanism. We confirmed that the C3–C4 finite element model with 60° facet was most susceptible to spinal cord injury without radiologic abnormality and that the bony pincers mechanism was dependent on facet joint inclination.

References

1. Pang D, Wilberger J. Spinal cord injury without radiographic abnormalities in children. *J Neurosurg* 1982;57:114–29.
2. Pang D, Pollack IF. Spinal Cord Injury without radiographic abnormality in children-the SCIWORA Syndrome. *J Trauma* 1989;29:654–64.
3. McCall T, Fassett D, Brockmeyer D. Cervical spine trauma in children: a review. *Neurosurg Focus* 2006;20:1–8.
4. Kothari P, Freeman B, Grevitt M, et al. Injury to the spinal cord without radiological abnormality (SCIWORA) in adults. *J Bone Joint Surg (Br)* 2000; 82–B:1034–7.
5. Ueta T. Cervical cord injuries without x-ray evidence of bony damages. Its pathology and treatment in the early stage. *Nichidoku-Iho* 2000;45:301–16.
6. Kawai H, Yabuno K. The injury mechanism of cervical cord injuries. The head and facial trauma related with cervical cord injuries. *J Osaka Med Assoc* 2003;37:34–8.
7. Teo EC, Ng HW. Evaluation of the role of ligaments, facets and disc nucleus in lower cervical spine under compression and sagittal moments using finite element method. *Med Eng Phys* 2001;23:155–64.
8. Maurel N, Lavaste F, Skalli W. A three-dimensional parameterized finite element model of the lower cervical spine. Study of the influence of the posterior facets. *J Biomech* 1997;30:921–31.
9. Kumaresan S, Yoganandan N, Pinter FA, et al. Finite element modeling of cervical laminectomy with graded facetectomy. *J Spinal Disord* 1997;10: 40–6.
10. Goel Vk, Clausen J. Prediction of load sharing among spinal components of a C5–C6 motion segment using the finite element approach. *Spine* 1998;23: 684–91.
11. Ng HW, Teo Ec. Nonlinear finite-element analysis of the lower cervical spine (C4–C6) under axial loading. *J Spinal Disord* 2001;14:201–10.
12. Pelker RR, Duranceau JS, Panjabi M. Cervical spine stabilization. A three-dimensional, biomechanical evaluation of rotational stability, strength, and failure mechanisms. *Spine* 1991;16:117–22.
13. Taylor AR, Blackwood W. Paraplegia in hyperextension cervical injuries with normal radiographic appearances. *J Bone Joint Surg* 1947;30:245–8.
14. Taylor AR. The mechanism of injury to the spinal cord in the neck without damage to the vertebral column. *J Bone Joint Surg* 1951;33–B:543–7.
15. Penning L. Some aspects of plain radiography of the cervical spine in chronic myelopathy. *Neurology* 1962;12:513–19.
16. Pearson AM, Ivancic PC, Ito S, et al. Facet joint kinematics and injury mechanisms during simulated whiplash. *Spine* 2004;29;390–7.
17. Kaneoka K, Ono K, Inami S, et al. Motion analysis of cervical vertebrae during whiplash loading. *Spine*1999;24:763–9.
18. Shea M, Edwards WT, White AA, et al. Validations of stiffness and strength along the human cervical spine. *J Biomech* 1991;24:95–107.
19. Heitplatz P, Hartle SL, Gentle CR. A 3-dimensional large deformation FEA of a ligamentous C4–C7 spine unit. Paper presented at: The Third International Symposium on Computer Methods in Biomechanics and Biomedical Engineering; 1998;387–94; Barcelona, Spain.
20. Moroney SP, Schultz AB, Miller JA, et al. Load-displacement properties of lower cervical spine motion segments. *J Biomech* 1988;21:767–79.
21. Yoganandan N, Kumaresan SC, Voo L, et al. Finite element modeling of the C4–C6 cervical spine unit. *Med Eng Phys* 1996;18:569–74.
22. Yoganandan N, Kumaresan SC, Voo L, et al. Finite element applications in human cervical spine modeling. *Spine* 1996;21:1824–34.
23. Panjabi M, Oxland T, Tanaka K, et al. Articular facets of the human spine. Quantitative three-dimensional anatomy. *Spine* 1993;18:1298–1310.

SPINE Volume 34, Number 3, pp E110–E114

Radiographic Analysis of the Cervical Spine in Patients With Retro-Odontoid Pseudotumors

Hirotaka Chikuda, MD,* Atsushi Seichi, MD,† Katsushi Takeshita, MD,* Naoki Shoda, MD,* Takashi Ono, MD,* Ko Matsudaira, MD,* Hiroshi Kawaguchi, MD,* and Kozo Nakamura, MD*

Study Design. A retrospective review of 10 consecutive patients with a noninflammatory retro-odontoid pseudotumor.

Objective. To examine the radiographic characteristics in patients with a retro-odontoid pseudotumor and to evaluate the efficacy of posterior fusion.

Summary of Background Data. A retro-odontoid pseudotumor, a reactive fibrocartilaginous mass, is known to develop after chronic atlantoaxial instability; however, one-third of the reported cases showed no overt atlantoaxial instability. The pathomechanism for such "atypical" cases remains unclear, although altered cervical motion secondary to ossification of the anterior longitudinal ligament (OALL) or severe spondylosis has been implicated.

Methods. We reviewed the charts and radiographs of 10 patients with a retro-odontoid pseudotumor who underwent surgery. Preoperative radiographs were evaluated for atlas-dens interval (ADI), presence of OALL, range of motion, and segmental motion adjacent to the atlantoaxial joint. Computed tomography was evaluated for degenerative changes of zygapophysial joints.

Results. There were 6 men and 4 women. Atlantoaxial instability (ADI >4 mm) was observed in 2 patients. ADI was less than 3 mm in 5 patients. Frequent association of OALL (6 patients) and marked decrease in C2 to C7 range of motion (mean, 17.6°; range, 3°–36°) were noted. Ankylosis of O-C1 was observed in 4 patients and C2 to C3 in 6. Severe degenerative change of C2 to C3 zygapophysial joint was observed in 4 patients. The patients underwent occipito-cervical fusion (9 patients) or direct removal of the pseudotumor (1 patient). Postoperative magnetic resonance imaging invariably demonstrated the mass regression.

Conclusion. Retro-odontoid pseudotumors were not always associated with radiographic atlantoaxial instability. Our data indicate that extensive OALL and ankylosis of the adjacent segments are risk factors for the formation of the pseudotumor. Retro-odontoid pseudotumors may develop as an "adjacent segment disease" after altered biomechanics of the cervical spine, especially those in the adjacent segments. Posterior fusion was effective even in cases without radiographic atlantoaxial instability.

Key words: retro-odontoid pseudotumor, atlantoaxial joint, adjacent segment, ossification of the anterior ligament, hyperostosis, myelopathy, range of motion, spinal fusion. **Spine 2009;34:E110–E114**

A noninflammatory retro-odontoid pseudotumor is a reactive fibrocartilaginous mass formed posterior to the odontoid process.[1–3] The retro-odontoid pseudotumor, a rare but increasingly recognized clinical entity, reportedly develops subsequent to chronic atlantoaxial instability. This view has been further supported by the regression of the mass after posterior fusion, which has become the mainstay of the treatment.[4–9] Although retro-odontoid pseudotumors have been frequently associated with atlantoaxial subluxation, we found that about one-third of the cases reported in the literature showed no overt atlantoaxial instability.[2,5,6,9–14] The pathomechanism for such atypical cases remains unclear, although modified stress distribution of the cervical spine, secondary to severe spondylosis or OALL, has been implicated.[15,16] Moreover, it has not been clarified whether posterior fusion aiming at spontaneous mass regression is similarly effective for the patients without radiographic atlantoaxial instability.

To further elucidate the underlying pathomechanism of the disease, we examined the radiographic characteristics of the cervical spine in patients with the retro-odontoid pseudotumors. Special attention was paid to the presence of OALL and the segmental motion adjacent to the atlantoaxial joint (O-C1, C2–C3). We also evaluated the efficacy of posterior fusion surgery.

Materials and Methods

After approval of institutional review board, we reviewed the clinical records of 140 patients who underwent surgery for upper cervical lesion at our department between 2000 and 2006. We identified 10 patients with retro-odontoid pseudotumors, and the radiographs of the 10 patients were examined. The diagnosis was made based primarily on magnetic resonance imaging (MRI) that revealed a mass lesion posterior to the odontoid process with substantial cord compression as evidenced by effacement of the subarachnoid space and indentation of the spinal cord. Masses were typically visualized as ranging from isointense to hypointense relative to spinal cord tissue on T1-weighted images and as hypointense regions on T2-weighted images. The diagnosis

From the *Department of Orthopaedic Surgery, Faculty of Medicine, the University of Tokyo, Tokyo, Japan; and †Department of Orthopaedic Surgery, Jichi Medical University, Jichi, Japan.
Acknowledgment date: March 27, 2008. Revision date: July 08, 2008. Acceptance date: July 21, 2008.
The manuscript submitted does not contain information about medical device(s)/drug(s).
No funds were received in support of this work. No benefits in any form have been or will be received from a commercial party related directly or indirectly to the subject of this manuscript.
This study was approved by the Tokyo University Medical Research Ethics Committee.
Address correspondence and reprint requests to Hirotaka Chikuda, MD, Department of Orthopaedic Surgery, Faculty of Medicine, the University of Tokyo, 7–3–1 Hongo, Bunkyo-ku, Tokyo 113-8655, Japan; E-mail: chikuda-tky@umin.ac.jp

Table 1. Scores of the Motor Functions of the Upper and Lower Extremities for Cervical Myelopathy Set by the Japanese Orthopaedic Association (JOA)

Motor function of the upper extremities (upper m-JOA)	
0	Cannot eat with a spoon
1	Can eat with a spoon, but not with chopsticks
2	Can eat with chopsticks, but to a limited degree
3	Can eat with chopsticks, but awkward
4	No disability
Motor function of the lower extremities (lower m-JOA)	
0	Cannot walk
1	Needs cane or aid on flat ground
2	Needs cane or aid only on stairs
3	Can walk without cane or aid, but slowly
4	No disability

was further confirmed by the radiology report. Specimen of the mass was available in 2 patients (patient 1 and 2). Subsequent histologic examination revealed fibrocartilage and degenerative ligamentous tissue. There was no recurrence of the mass lesion during the follow-up period. Inflammatory granulation of the synovium associated with rheumatoid arthritis and retro-odontoid reactive lesions associated with pseudarthrosis of the dens fracture were excluded from this study. All patients had symptoms of progressive myelopathy: hyperreflexia, positive pathologic reflexes, motor weakness in the upper and lower extremities, clumsiness in hands, and gait disturbance. Neurologic status of the patients was evaluated before surgery and at the last follow-up by a senior author (A.S.). Motor function was rated using the motor function scores of the upper and lower extremities for cervical myelopathy set by the Japanese Orthopedic Association (upper and lower m-JOA score) (Table 1). A full score "4" indicates normal function.

All radiographs were viewed using our institution's digital radiography software (Centricity Web-J software ver.1.6.11; GE Yokogawa Medical Systems, Tokyo, Japan). The measurement of the radiographs was performed independently by 2 spine surgeons (H.C. and N.S.) with the program's digital measuring tool. The results of the 2 reviewers were averaged. The atlas-dens interval (ADI) was measured on preoperative flexion-extension radiographs. The atlantoaxial instability was defined as ADI >4 mm, according to the criteria described by White and Panjabi.[17] Lateral radiographs and sagittal computed tomography (CT) reconstructions were evaluated for the presence of OALL. OALL was defined as bony mass anterior to the vertebrae bridging over 2 or more intervertebral disc spaces. Range of motion (ROM) was measured on preoperative flexion-extension radiographs. The representative lines used for the measurement were as follows: the McGregor line, the line passing through the centers of anterior and posterior arches of the atlas, and the line parallel to the endplate of vertebrae. The mobility of each segment was determined by measuring the difference between 2 corresponding points on the tips of the spinous processes on flexion *versus* extension. Ankylosis was defined as absence of motion on both flexion and extension radiographs. CT reconstructions were further evaluated for degenerative change or fusion of the zygapophysial joints. To assess the regression of the pseudotumor, follow-up MRI obtained 1 year after surgery was reviewed. Maximal thickness of the retro-odontoid soft tissue was measured on preoperative and postoperative MRI in T2-weighted sagittal view. Interobserver reliability of radiographic measurement was assessed with inter class coefficient. All statistics were calculated using SPSS, version 13.0 (SPSS Inc., Chicago, IL).

■ Results

There were 6 men and 4 women with a mean age at surgery of 71 years (range, 58–82 years). Mean follow-up was 30 months (range, 12–84 months). Maximal thickness of the retro-odontoid soft tissue was 9.4 ± 1.3 mm (mean ± SD; range, 7.6-11.4 mm). On examination of the radiographic characteristics (Table 2), ADI averaged 3.4 ± 1.9 mm (mean ± SD) in flexion and 1.8 ± 0.9 mm in extension. Only 2 patients showed overt atlantoaxial instability (ADI >4 mm). ADI was less than 3 mm in 5 patients (Figure 1). We found extensive OALL in 6 patients: C2 to C7 in 4 patients, and C3 to C7 and C3 to C5 in 1 patient each. When ROM of the cervical spine was examined, marked decrease in subaxial (C2–C7)

Table 2. Radiographic Characteristics of the Cervical Spine

		ADI (mm)			ROM (°)		Segmental Motion (°)	
Patient No.	Age (Yr), Sex	Flexion	Extension	OALL	O-C2	C2–C7	O-C1	C2–C3
1	58, M	7.0 ± 0.1	3.2 ± 0.3	C2–C7	30 ± 3.0	6 ± 1.5	7 ± 1.0	10 ± 3.0
2	67, F	6.6 ± 0.6	6.2 ± 0	C3–C5	14 ± 9.1	28 ± 3.9	None*	None
3	72, F	3.5 ± 0.7	1.0 ± 0.1	C2–C7	32 ± 0.9	7 ± 0.6	6 ± 1.1	8 ± 3.6
4	71, M	3.4 ± 0.1	1.5 ± 0	—	17 ± 0.4	23 ± 0.7	None	3 ± 0.2
5	82, M	3.3 ± 0.4	2.1 ± 0.3	C2–C7	18 ± 5.3	5 ± 4.9	8 ± 0.1	None
6	81, M	2.8 ± 0.6	1.5 ± 1.0	C2–C7	35 ± 1.7	22 ± 2.6	5 ± 0.8	None†
7	73, F	2.7 ± 0.1	1.9 ± 0.4	—	24 ± 1.1	35 ± 0.2	None	5 ± 2.5†
8	73, M	2.0 ± 0.6	1.7 ± 0.3	C3–C7	8 ± 0.3	11 ± 2.4	None	None†
9	71, F	2.0 ± 0.3	1.7 ± 0.9	—	28 ± 6.2	36 ± 2.8	4 ± 1.6	None
10	64, M	1.0 ± 0.1	0 ± 0	—	24 ± 2.7	3 ± 3.5	15 ± 3.1	None†

Data are shown as mean ± SD. ICC values for radiographic measurement were as follows: ADI in flexion, 0.97; ADI in extension, 0.98; O-C2 ROM, 0.88; C2–C7 ROM, 0.98; O-C1 ROM, 0.96; and C2–C3 ROM, 0.87. The 2 reviewers were in accord regarding the categorical items including presence of OALL and segmental ankylosis.
*Atlanto-occipital assimilation.
†Severe spondylosis of the C2–C3 zygapophyseal joint.

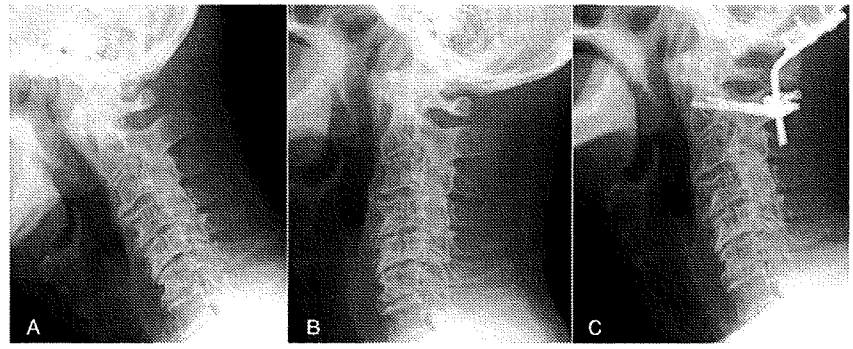

Figure 1. Preoperative radiographs of a 73-year-old man (patient 8) revealed extensive OALL. Atlantoaxial instability was not evident in flexion (**A**) and extension (**B**). The patient underwent O-C2 fusion with C1 laminectomy (**C**).

ROM was noted (mean, 17.6°; range, 3°-36°), especially in the patients with OALL. Further analysis of the segmental motion revealed ankylosis in O-C1 in 4 patients (including 1 patient with atlanto-occipital assimilation) and C2–C3 in 6 patients. Furthermore, CT revealed severe degenerative changes of the C2 to C3 zygapophysial joint in 4 patients (Figure 2).

All but 1 patient were treated with posterior occipitocervical fusion using pedicle screws (Table 3). Surgical procedures included O-C2 fusion (6 patients), O-C4 fusion(3 patients), and direct tumor resection by the lateral approach(1 patient). Additional C1 laminectomy was performed in all patients who underwent posterior fusion except 1 patient in whom adequate decompression was confirmed with intraoperative ultrasonography. There was no documented complication during perioperative period except that 1 patient had acute coronary syndrome, which required subsequent intervention. Neurologic status improved after surgery in all but 1 patient who was suffering from esophageal cancer. Preoperative upper m-JOA score (median, 2; range, 1–3) improved after surgery (median, 3.5; range, 1–4). Similarly, lower m-JOA score (median, 2; range, 1–3) also improved after surgery (median, 3; range, 2–4). Follow-up MRI was available in 8 patients. In the remaining 2 patients, deteriorated health status due to unrelated diseases (esophageal cancer and pneumonia, respectively) precluded further study. MRI revealed the regression of the pseudotumors in all patients and decompression of the spinal cord (Figure 3). Regression of the pseudotumors was confirmed by emergence of the subarachnoid space in postoperative MRI and further evidenced by reduction in thickness of the retro-odontoid soft tissue (3.4 ± 0.8 mm; range, 2.3-4.7 mm).

■ Discussion

Our study had 3 main findings. First, we have shown that the retro-odontoid pseudotumors can develop without overt atlantoaxial instability. Second, we found marked decrease in subaxial ROM, mainly because of extensive OALL. Furthermore, most of the patients had ankylosis of O-C1 or C2 to C3, the segments adjacent to the atlantoaxial joint. Finally, spontaneous mass regression occurred after posterior fusion even in the absence of radiographic atlantoaxial instability.

The retro-odontoid pseudotumor has been generally considered as a rare sequela of atlantoaxial subluxation. In the postulated view on its pathomechanism, preexisting atlantoaxial instability was presumed to cause repeated tear and subsequent hypertrophy of the transverse ligament,[4,16] thus leading to the formation of the pseudotumor. The current study, however, revealed that the retro-odontoid pseudotumors were not necessarily associated with overt atlantoaxial instability. This finding indicates a different view on the formation of the pseudotumor: In the first place, excessive stress concentration to the atlantoaxial complex, due to altered biomechanics of the cervical spine, may repeatedly cause damage to the transverse ligament. A reactive mass may develop gradually after cycles of repetitive injuries to the ligament and reparative process. Although atlantoaxial subluxation might ensue from further attenuation of the

Figure 2. Sagittal (**A**) and axial (**B**) CT reconstructions (both from patient 8) demonstrated severe spondylosis in bilateral C2 to C3 zygapophysial joints.

Table 3. Outcome of Surgical Treatment

Patient No.	Surgery	Preoperative m-JOA		Postoperative m-JOA		Outcome	Follow-up MRI
		Upper	Lower	Upper	Lower		
1	Partial removal, O-C2 fusion, C1 laminectomy	1	1	2	2	Improved	Regression
2	Direct removal	2	1	4	4	Improved	Extirpated
3	O-C4 fusion, C1 laminectomy	1	2	3	3	Improved	N.A.*
4	O-C2 fusion, C1 laminectomy	1	2	3	3	Improved	Regression
5	O-C4 fusion, C1 laminectomy	1	2	1	2	Unchanged	N.A.*
6	O-C2 fusion, C1 laminectomy, C3–C7 laminoplasty	2	2	3	2	Improved	Regression
7	O-C2 fusion, C3–C7 laminoplasty	3	2	4	4	Improved	Regression
8	O-C2 fusion, C1 laminectomy	3	3	4	4	Improved	Regression
9	O-C2 fusion, C1 laminectomy	2	2	4	4	Improved	Regression
10	O-C4 fusion, C1–C2 laminectomy	2	2	4	3	Improved	Regression

*Deterioration of the patient's condition due to unrelated diseases precluded the follow-up MRI study.
Upper, indicates upper extremities; Lower, lower extremities; N.A., not available.

ligamentous structure, atlantoaxial instability should be viewed as a consequence of the degeneration process, not a prerequisite for the formation of the pseudotumor.

We found that extensive OALL was highly prevalent in patients with retro-odontoid pseudotumors. Modified stress distribution secondary to extensive OALL has been implicated in the literature as possible pathomechanism. Jun *et al* reported a case with diffuse idiopathic skeletal hyperostosis and attributed its cause to loss of mobility of subaxial segments and the secondary transfer of mechanical stress to the atlantoaxial segment.[16] Patel *et al* reported 5 patients of a retro-odontoid mass associated with Forestier disease, speculating that multilevel subaxial fusion because of OALL coupled with the mobility of the craniovertebral joint complex plays a pivotal role in the development of the mass.[15] In line with these reports, the current study demonstrated extensive OALL and marked decrease in subaxial ROM in patients with a retro-odontoid pseudotumor. Our data indicate that altered biomechanics of the cervical spine because of OALL plays a role in formation of the retro-odontoid pseudotumor.

Ankylosis of the segments adjacent to the atlantoaxial joint was another characteristic finding associated with retro-odontoid pseudotumors. Loss of mobility at the adjacent segment is known to contribute to increased risk of atlantoaxial dysfunction in other chronic condi-

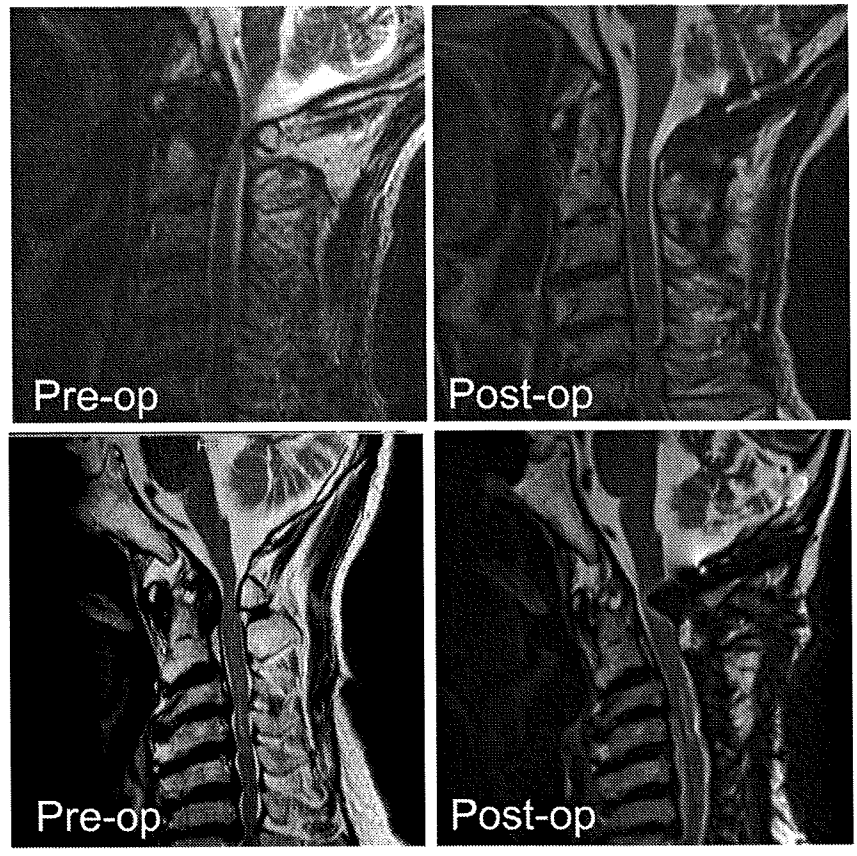

Figure 3. Preoperative and postoperative T2-weighted MR images of patient 8 (upper panels) and patient 6 (lower panels). Spontaneous regression of the mass lesion occurred after posterior fusion.

tions. In patients with Klippel-Feil syndrome, in which the C2 to C3 is the most commonly fused level, subsequent stress transfer at the C1 to C2 segment has been suggested as a risk factor for atlantoaxial instability. Shen *et al* have shown that occipitalization combined with a fused C2 to C3 segment results in the greatest amount of atlantoaxial instability in patients with Klippel-Feil syndrome.[18] Our results suggest that the altered dynamics of the cervical spine, especially those in the adjacent segments —O-C1 and C2 to C3—play a crucial role in the development of the retro-odontoid pseudotumor, indicating that the mass develops as an adjacent segment disease.

Optimal treatment for a retro-odontoid pseudotumor that is not associated with atlantoaxial instability has not been established, although transoral removal has usually been employed in such a case. In this study, 3 types of surgical procedures were used: extirpation of the mass, O-C2 fusion, and O-C4 fusion. We performed extirpation only in the earlier period when posterior fusion was not known to be effective. Afterward, we used posterior fusion as the treatment of choice. We preferred occipito-cervical fusion to C1 to C2 fusion because of ample space for bone grafting even after the resection of C1 posterior arch, which was performed in most cases. We usually extended fusion down to C4 when safety of inserting C2 pedicle screws was in doubt because of the anatomic limitations such as high riding vertebral artery, identified by preoperative planning using CT navigation system. In the current study, we have shown that posterior fusion invariably produced mass regression even in cases without radiographic atlantoaxial instability. This previously undocumented finding may be attributable to the fact that posterior fusion greatly reduces stress concentration to the atlantoaxial junction. Considering that the reactive mass develops as an adjacent segment disease, relieving mechanical stress at the atlantoaxial junction is a reasonable strategy for preventing further progression of the disease. Our data indicate that posterior fusion is the treatment of choice even for cases without overt atlantoaxial instability.

There are several limitations to the present study. Although this is the largest case series, we need to examine more cases to determine the precise incidence of the radiographic characteristics we mentioned. Moreover, a cohort or case-control study is required to further demonstrate the cause-effect relationship of the putative risk factors we discussed in the present study. Retro-odontoid pseudotumors occur only in a fraction of population with OALL or having ankylosis of O-C1 or C2 to C3, which may be partly attributable to variable biologic responses of the ligamentous tissue among the individuals. Further studies are needed to clarify the role of other biologic or genetic factors that predispose patients to development of retro-odontoid pseudotumors.

■ Conclusion

Retro-odontoid pseudotumors were not always associated with radiographic atlantoaxial instability. Our results suggest that extensive OALL and ankylosis of the adjacent segments are risk factors for the formation of pseudotumors. The retro-odontoid pseudotumors may develop as an adjacent segment disease after altered biomechanics of the cervical spine, especially those in the adjacent segments. Posterior fusion is the treatment of choice even for cases without radiographic atlantoaxial instability.

■ Key Points

- Retro-odontoid pseudotumors were not necessarily associated with radiographic atlantoaxial instability.
- Subaxial fusion due to OALL and ankylosis of the adjacent segments (O-C1, C2–C3) may be risk factors for the formation of the pseudotumor.
- Posterior fusion resulted in spontaneous regression of the pseudotumor even in cases without radiographic atlantoaxial instability.

References

1. Oohori Y, Seichi A, Kawaguchi H, et al. Retroodontoid pseudotumor resected by a high cervical lateral approach in a rheumatoid arthritis patient: a case report. *J Orthop Sci* 2004;9:90–3.
2. Crockard HA, Sett P, Geddes JF, et al. Damaged ligaments at the craniocervical junction presenting as an extradural tumour: a differential diagnosis in the elderly. *J Neurol Neurosurg Psychiatr* 1991;54:817–21.
3. Sze G, Brant-Zawadzki MN, Wilson CR, et al. Pseudotumor of the craniovertebral junction associated with chronic subluxation: MR imaging studies. *Radiology* 1986;161:391–4.
4. Yoshida MT, Kawakami M, Natsumi K, et al. Retro-odontoid pseudotumor associated with chronic atlanto-axial instability. *Rinsho Seikei Geka* 1995; 30:395–402 [in Japanese].
5. Yamashita K, Aoki Y, Hiroshima K. Myelopathy due to hypoplasia of the atlas: a case report. *Clin Orthop Relat Res* 1997:90–3.
6. Yamaguchi I, Shibuya S, Arima N, et al. Remarkable reduction or disappearance of retroodontoid pseudotumors after occipitocervical fusion: report of three cases. *J Neurosurg Spine* 2006;5:156–60.
7. Jun BY. Complete reduction of retro-odontoid soft tissue mass in os odontoideum following the posterior C1–C2 tranarticular screw fixation. *Spine* 1999;24:1961–4.
8. Lagares A, Arrese I, Pascual B, et al. Pannus resolution after occipitocervical fusion in a non-rheumatoid atlanto-axial instability. *Eur Spine J* 2006;15: 366–9.
9. Lansen TA, Kasoff SS, Tenner MS. Occipitocervical fusion for reduction of traumatic periodontoid hypertrophic cicatrix: case report. *J Neurosurg* 1990;73:466–70.
10. Rabadan AT, Sevlever G. Hypertrophic atlantoaxial ligaments: an unusual cause of compression of the upper spinal cord. *J Neurol Neurosurg Psychiatr* 2000;68:116–17.
11. Komatsu Y, Shibata T, Yasuda S, et al. Atlas hypoplasia as a cause of high cervical myelopathy: case report. *J Neurosurg* 1993;79:917–19.
12. Chen TY, Lui TN. Retrodental fibrocartilaginous mass: report of a case. *Spine* 1997;22:920–3.
13. Sato K, Kubota T, Takeuchi H, et al. Atlas hypoplasia associated with nontraumatic retro-odontoid mass. *Neurol Med Chir (Tokyo)* 2006;46:202–5.
14. Suetsuna F, Narita H, Ono A, et al. Regression of retroodontoid pseudotumors following C-1 laminoplasty: report of three cases. *J Neurosurg Spine* 2006;5:455–60.
15. Patel NP, Wright NM, Choi WW, et al. Forestier disease associated with a retroodontoid mass causing cervicomedullary compression. *J Neurosurg* 2002;96:190–6.
16. Jun BY, Yoon KJ, Crockard A. Retro-odontoid pseudotumor in diffuse idiopathic skeletal hyperostosis. *Spine* 2002;27:E266–70.
17. White AA, Panjabi, MM. *Clinical Biomechanics of the Spine.* 2nd ed. Philadelphia: Lippincott Williams and Wilkins; 1990.
18. Shen FH, Samartzis D, Herman J, et al. Radiographic assessment of segmental motion at the atlantoaxial junction in the Klippel-Feil patient. *Spine* 2006;31:171–7.